Available online at www.sciencedirect.com
SCIENCE DIRECT®
Marine Geology 205 (2004) 29–58
MARINE GEOLOGY
INTERNATIONAL JOURNAL OF MARINE GEOLOGY, GEOCHEMISTRY AND GEOPHYSICS
www.elsevier.com/locate/margeo

Glacial–interglacial (MIS 1–10) migrations of the Subtropical Front across ODP Site 1119, Canterbury Bight, Southwest Pacific Ocean

R.M. Carter [a,b,*], P.R. Gammon [a], L. Millwood [c]

[a] *Department of Geology and Geophysics, University of Adelaide, Adelaide, SA, Australia*
[b] *Marine Geophysical Laboratory, James Cook University, Townsville, Qld, Australia*
[c] *Department of Geology, University of Texas, Arlington, TX, USA*

Received 31 July 2002; received in revised form 12 June 2003; accepted 26 January 2004

Abstract

Ocean Drilling Program (ODP) Site 1119 is located at water depth 395 m near the subtropical front (STF; here represented by the Southland Front), just downslope from the shelf edge of eastern South Island, New Zealand. The upper 86.19 metres composite depth (mcd) of Site 1119 sediment was deposited at an average sedimentation rate of 34 cm/kyr during Marine Isotope Stages (MIS) 1–8 (0–252 ka), and is underlain across a ~25 kyr intra-MIS 8 unconformity by MIS 8.5–11 (277–367 ka) and older sediment deposited at ~14 cm/kyr. A time scale is assigned to Site 1119 using radiocarbon dates for the period back to ~39 ka, and, prior to then, by matching its climatic record with that of the Vostok ice core, which it closely resembles. Four palaeoceanographic proxy measures for surface water masses vary together with the sandy-muddy, glacial–interglacial (G/I) cyclicity at the site. Interglacial intervals are characterised by heavy $\delta^{13}C$, high colour reflectance (a proxy for carbonate content), low γ-ray (a proxy for clay content) and light $\delta^{18}O$; conversely, glacial intervals exhibit light $\delta^{13}C$, low reflectance, high γ-ray and heavy $\delta^{18}O$ signatures. Early interglacial intervals are represented by silty clays with 10–105-cm-thick beds of sharp-based (*Chondrites*-burrowed), shelly, graded, fine sand. The sands are rich in foraminifera, and were deposited distant from the shoreline under the influence of longitudinal flow in relatively deep water. Glacial intervals comprise mostly micaceous silty clay, though with some thin (2–10 cm thick) sands present also at peak cold periods, and contain the cold-water scallop *Zygochlamys delicatula*. Interglacial sandy intervals are characterised by relatively low sedimentation rates of 5–32 cm/kyr; cold climate intervals MIS 10, 6 and 2 have successively higher sedimentation rates of 45, 69 and 140 cm/kyr. Counter-intuitively, and forced by the bathymetric control of a laterally-moving shoreline during G/I and I/G transitions, the 1119 core records a southeasterly (seaward) movement of the STF during early glacial periods, accompanied by the incursion of subtropical water (STW) above the site, and northwesterly (landward) movement during late glacial and interglacial times, resulting in a dominant influence then of subantarctic surface water (SAW). The history of passage of these different water masses at the site is clearly delineated by their characteristic $\delta^{13}C$ values. The intervals of thin, graded sands–muds which occur within MIS 2–3, 6, 7.4 and 10 indicate the onset at times of peak cold of intermittent bottom currents caused by strengthened and expanded frontal flows along the STF, which at such times lay near Site 1119 in close proximity to seaward-encroaching subantarctic

* Corresponding author. Tel.: +61-747814397; Fax: +61-747814334.
E-mail address: bob.carter@jcu.edu.au (R.M. Carter).

0025-3227/04/$ – see front matter
doi:10.1016/S0025-3227(04)00017-9

waters within the Bounty gyre. In common with other nearby Southern Hemisphere records, the cold period which represents the last glacial maximum lasted between ~23–18 ka at Site 1119, during which time the STF and Subantarctic Front (SAF) probably merged into a single intense frontal zone around the head of the adjacent Bounty Trough.

Keywords: Ocean Drilling Program (ODP); Subtropical Front (STF); Subtropical Water (STW); Subantarctic Water (SAW); glacial–interglacial change; Southland Front; cyclic sedimentation; sea level; New Zealand; Southwest Pacific

1. Introduction

Ocean Drilling Program (ODP) Site 1119 is located at a water depth of 395 m on the upper continental slope, east of South Island, New Zealand (Fig. 1). The drillhole penetrated a 0–86.19 metres composite depth (mcd) interval of prograding mud foresets (Fig. 2), underlain by 400+ m of Neogene sediment drifts deposited in waters of intermediate depth (~500–1200 m) (Fulthorpe and Carter, 1991; Lu et al., 2003). At present, the site lies just seawards of the Subtropical Front (STF), which is represented off eastern South Island by the Southland Front (Fig. 3) (Burling, 1961; Chiswell, 1996). The front separates dominantly warm, saline subtropical and mixed water of the Southland Current, which bathes the shelf and upper slope to the west, from cold, fresher, oceanic subantarctic water to the east (Heath, 1981). The unusual northeasterly orientation of the front here results from the fact that South Island, New Zealand, straddles the mid-latitudes in which the STF is developed. Zonal segments of the STF at ~45°S in the Tasman Ocean and ~43°S in the Southwest Pacific are thus connected along the Southland Front, the disposition of which reflects the bathymetric steering of the water masses involved around South Island. Site 1119 today also lies near the upper edge of a seabed zone of mid-slope sediment drift deposition, which is induced at depths of ~400–1200 m by slope-parallel currents within northward-travelling Subantarctic Mode Water (SAMW) and Antarctic Intermediate Water (AAIW) (Carter et al., 1996).

This paper addresses three main issues, based on the record of the upper 100 mcd of the Site 1119 core (Marine Isotope Stages (MIS) 1–11; 0–370 ka). First, the assembly of an improved time scale from that available immediately after drilling (Carter et al., 1999), prepared using Accelerator Mass Spectrometry (AMS) radiocarbon dates and by matching four palaeoceanographic proxies, and especially the γ-ray record, between Site 1119 and the Antarctic climatic record represented in the Vostok ice core. Second, an interpretation of the four proxies in terms of the changing climate and oceanography of the New Zealand sector of the Southwest Pacific Ocean since 370 ka. And third, a discussion of the controls on the deposition of the major glacial and interglacial sediment facies at Site 1119, and their interpretation in terms of oscillations in the position of the STF.

2. Methods and materials

Two main holes, B and C, were cored at Site 1119 to the 150–160 mbsf depth of refusal of the advanced piston corer (APC). Hole 1119C was then continued to TD 494.8 mbsf using the extended core barrel (XCB). Henceforward, all depths are given in mcd, based upon the spliced core record between all holes which was created during the cruise (Weedon and Harris, in: Carter et al., 1999, fig. F19). The section studied comprises all of Unit I and a small part of upper Unit II of Carter et al. (1999). The boundary between these two units was chosen to correspond to a visible seismic unconformity between clinoform slope foresets above and drift deposits below. In keeping with that intention, we adjust the location of the Unit I/II boundary here to 86.19 mcd, which is significantly shallower than the 94 mcd

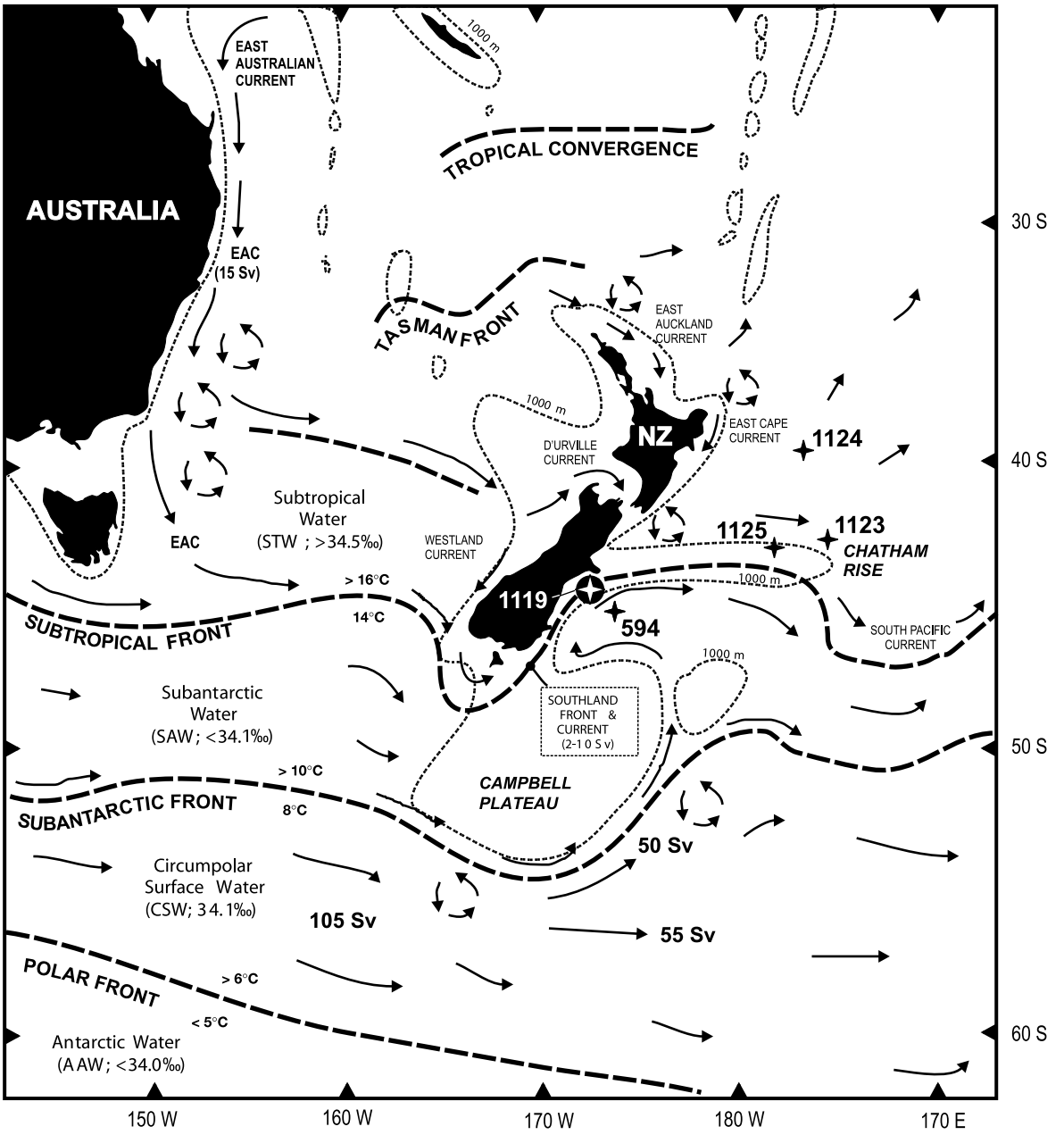

Fig. 1. Locality map of the Southwest Pacific region, showing the location of ODP Site 1119, and nearby sites, with respect to South Island, New Zealand, and to the major modern oceanographic fronts and surface current flows.

(88 mbsf) depth that was estimated from shipboard data alone. Pre-Holocene sedimentation rates range between ~14–141 cm/kyr over MIS 2–7, above the unconformity, and ~10–45 cm/kyr over MIS 8–11, below. The occurrence within the succession of sands, shelly intervals and the cold-climate scallop *Zygochlamys delicatula* are summarised in Table 1.

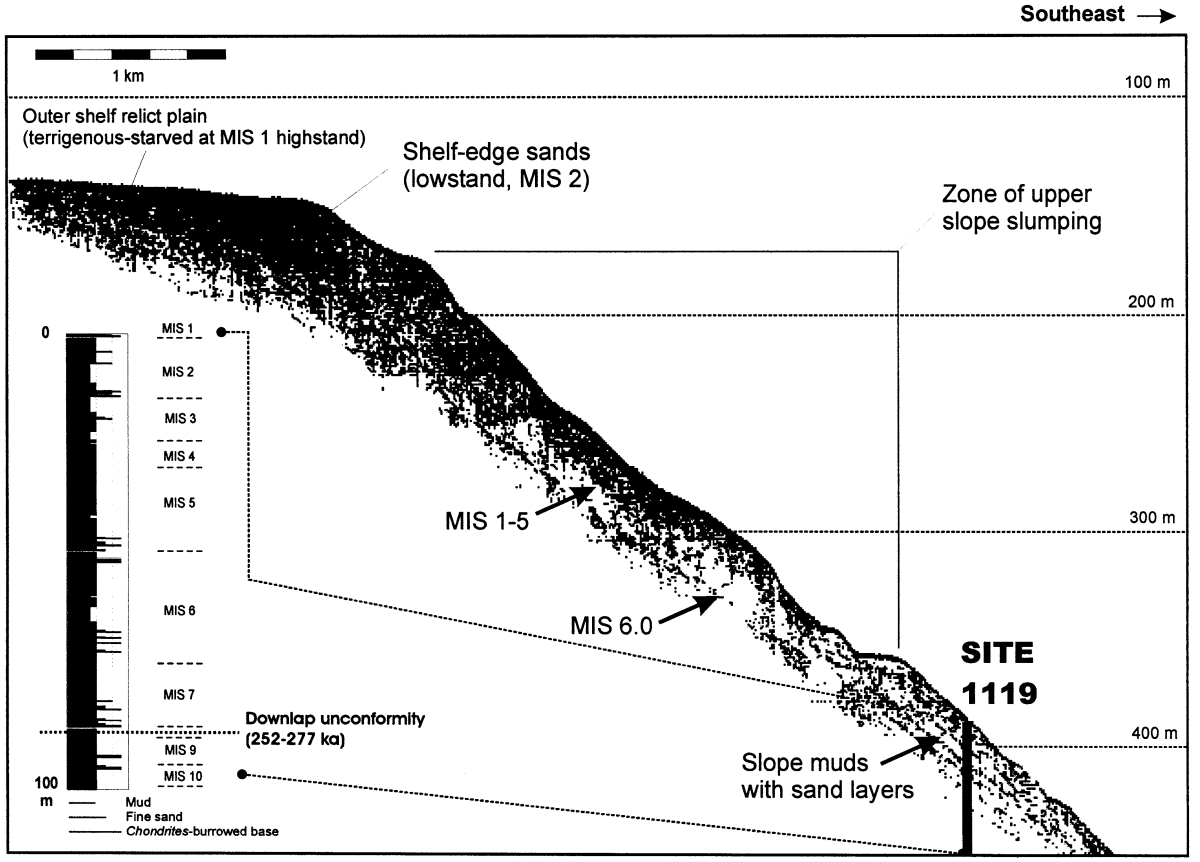

Fig. 2. 3.5-kHz profile through Site 1119, normal to the shelf edge (after Carter et al., 1999). Inset (left), lithological log for the upper 100 mcd of the core.

2.1. Natural γ-ray intensity

Natural γ-ray intensity was measured with the ODP shipboard multi-sensor track (MST) assembly, with data points recorded at 15-cm intervals along the whole-round core after temperature stabilisation. A spliced, composite γ-ray record of data from the A (mudline), B and C cores was then assembled against the mcd scale. As plotted in Figs. 4 and 5, this record has a resolution of ~130–1000 years above the downlap unconformity and ~360–1500 years below.

2.2. Colour reflectance

The colour reflectance (400–700 nm) record, which serves as a proxy for carbonate content, was compiled post-cruise at the ODP–TAMU core repository by L. Millwood, using a Minolta spectrophotometer and taking measurements at average intervals of ~10 cm along the archival half of split core 1119-C. The reflectance record was calibrated to measured carbonate samples from the core, using a regression model, and the data are plotted accordingly on a percentage-carbonate scale (Figs. 4 and 5). Fuller details of the analytical methods used are given in Millwood et al. (2003). The data have a resolution of ~90–630 years above the unconformity and ~240–1000 years below.

2.3. Stable isotope measurement

Samples for stable isotope measurement were

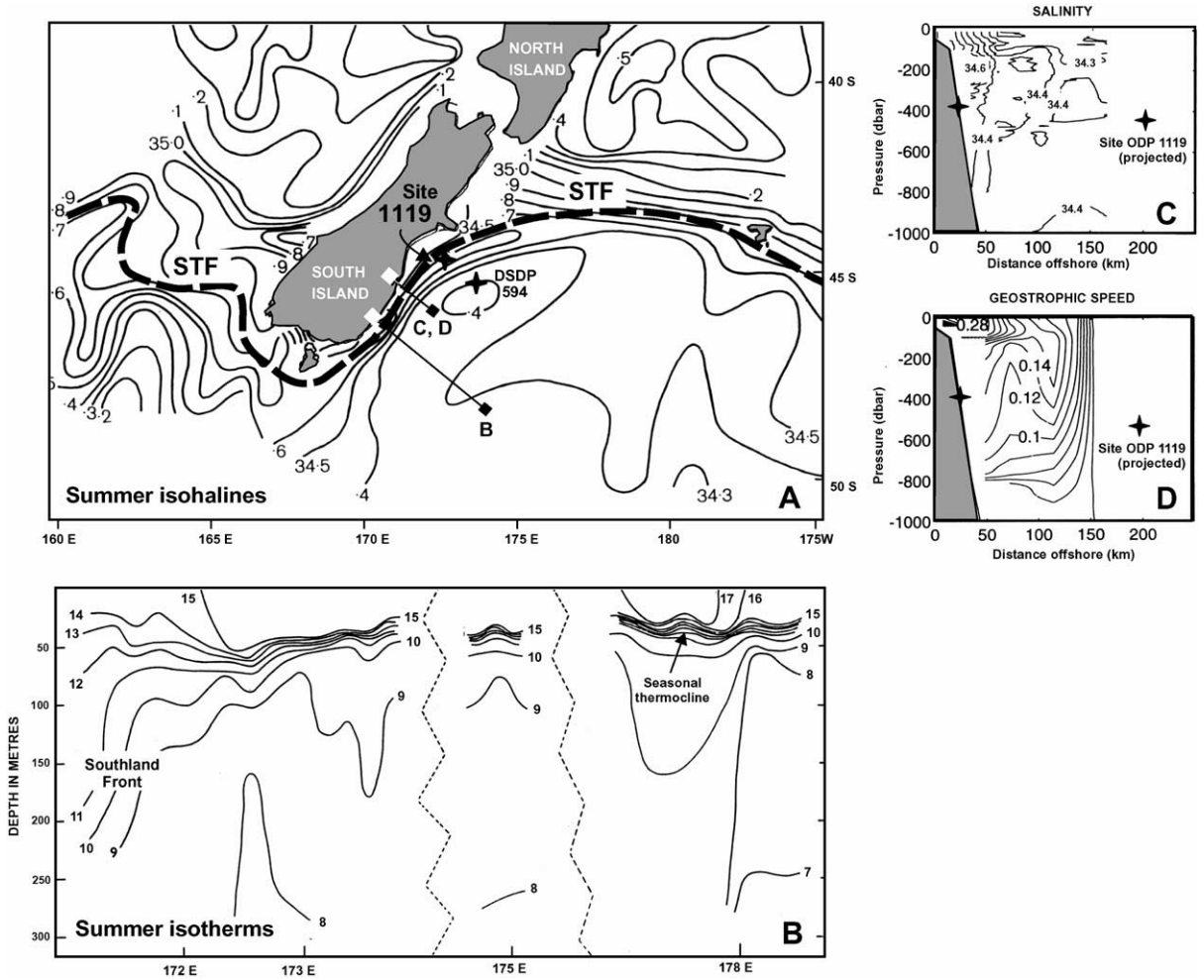

Fig. 3. Oceanographic setting of sites ODP 1119 and DSDP 594. (A) Surface map of the summer isohalines for the Southwest Pacific region (after Heath, 1985), showing location of sites 1119 and 594, locations of profiles B, C and D, and the position of the Subtropical Front (STF). (B) Profile normal to the Otago coastline of summer isotherms for the upper 300 m; note the well developed seasonal thermocline, and the presence of the STF (=Southland Front; after Garner and Ridgway, 1965). (C,D) Profiles of salinity and calculated geostrophic current across the eastern South Island shelf edge; note the presence of strong frontal features, including the tongue of saline water which hugs the upper slope between 200 and 400 m (C), and the core of the shallow water Southland Current directly inboard from Site 1119 (D) (after Chiswell, 1996).

taken at ~1-m intervals over the top 50 m of the core (MIS 1–5), and ~3–5-m intervals over the interval 50–100 m (MIS 6–11). Accordingly, the stable isotope curves have a resolution of ~1 ky for MIS 1–5, and ~2–5 ky for MIS 6–10. Planktic foraminifera were prepared by separation from the hemipelagic mudstone by sieving through 63-μm mesh size, picking, gentle ultrasonification in 5% hydrogen peroxide, and rinsing in de-ionised water. Generally 4–6 specimens of *Globigerina bulloides* were analysed per sample. However, some carbonate-poor samples only yielded 1–4 tests for analysis. In all samples, overly large, small, stained or damaged specimens were rejected. The carbonate isotope samples were analysed by P. Gammon at the Department of Geology and Geophysics, University of Adelaide, using an automated on-line 'Micromass Isocarb'

Table 1
Summary table of sand beds, shell concentrations, and occurrences of the cold-water scallop *Zygochlamys delicatula* in the upper 100 mcd of cores 1119B and C

Sand bed No.	Bed type	Nature of bed base	Site 1119 core	Base (mbsf)	Base (mcd)	Adopted (mcd)	Thickness (cm)	Adopted (cm)	Age (ka)	MIS
S-1	Sand	*Chondrites*	A	0.34	0.34	Probable loss of ~12 cm from top of core			9.5	1
S-1	Sand	*Chondrites*	B	0.42	0.46	0.46	22	22	9.5	1
S-1	Sand	*Chondrites*	C	0.13	0.37	Probable loss of ~29 cm from top of core			9.5	1
Basal Holocene diastem (0.46 mcd, ~9.0–12.0 ka)										
Zygochlamys			B	2.00	2.04	2.04			15.1	2
S-2a	Shells		A	3.90	3.90	3.91	5	5	16.5	2
S-2a	Shells		B	3.87	3.91	3.91	4	5	16.5	2
S-2a	Shells		C	3.76	3.92	3.91	5	5	16.5	2
S-2b	Shells		B				not seen			
S-2b	Shells		C	6.24	6.40	6.40	5	5	18.2	2
Zygochlamys			B		7.69	7.93			19.3	2
S-2c	Sand	*Chondrites*	B	12.40	12.64	12.65	15	15	22.7	2
S-2c	Sand		C	12.90	12.66	12.65	15	15	22.7	2
Zygochlamys			C	12.93	12.69	12.69			22.7	2
S-2d	Sand		B	12.62	12.86	12.88	4	4	22.8	2
S-2d	Sand		C	13.14	12.90	12.88	4	4	22.8	2
Zygochlamys			C	13.14	12.90	12.88	in S-2d		22.8	2
S-2e	Shells		B	12.76	13.00	13.01	4	3	22.9	2
S-2e	Shells		C	13.27	13.03	13.01	2	3	22.9	2
Zygochlamys			B	12.85	13.09	13.09			23.0	3
S-3a	Shells	*Chondrites*	B	13.42	13.66	13.63	5	6	23.4	3
S-3a	Shells		C	13.83	13.59	13.63	8	6	23.4	3
Zygochlamys			B	13.40	13.64	13.63	in S-3a		23.4	3
Zygochlamys			C	13.83	13.59	13.63	in S-3a		23.4	3
Zygochlamys			C	14.35	14.11	14.11			23.7	3
Zygochlamys			B	15.44	16.68	16.68			31.9	3
S-3b	Sand		B	16.47	17.10	18.34	10	10	38.1	3
S-3b	Sand		C				in core gap			
S-3c	Shells		B	17.46	18.70	18.71	5	5	39.5	3
S-3c	Shells		C	19.01	18.73	18.71	5	5	39.5	3
Zygochlamys			C	18.98	18.71	18.71	in S-3c		39.5	3
Zygochlamys			C	19.16	18.88	18.88			40.0	3
Zygochlamys			C	27.90	27.94	27.94			67.7	4
S-5a	Sand		B				in core gap			
S-5a	Sand	*Chondrites*	C	43.95	44.95	44.95	15	15	121.6	5.5
S-5b	Sand		B	43.47	46.45	46.43	5	5	127.4	5.5
S-5b	Sand	*Chondrites*	C	45.41	46.41	46.43	5	5	127.4	5.5
S-5c	Sand	*Chondrites*	B	44.60	47.58	47.58	20	20	132.0	5.5
S-5c	Sand		C				in core gap			
Inferred MIS 6–5 diastem (47.58 mcd, ~132–135 ka)										
S-6a	Sand	*Chondrites*	B	45.20	48.18	48.18	3	3	138.0	6.2
S-6a			C				in core gap			
S-6b	Sand	*Chondrites*	B	45.54	48.52	48.52	3	3	139.7	6.2
S-6b			C				in core gap			
S-6c	Shells		B	45.83	48.81	48.81	4	4	141.1	6.2
S-6c			C				in core gap			
S-6d	Shells	*Chondrites*	B	45.91	48.89	48.88	2	2	141.5	6.2
S-6d	Shells	*Chondrites*	C	46.61	48.87	48.88	2	2	141.5	6.2
S-6e	Sand	*Chondrites*	B	46.11	49.09	49.11	7	7	142.6	6.3
S-6e	Sand	*Chondrites*	C	46.87	49.13	49.11	7	7	142.6	6.3
S-6f	Sand	*Chondrites*	B	46.62	49.60	49.62	7	6	145.2	6.3
S-6f	Sand	*Chondrites*	C	47.38	49.64	49.62	5	6	145.2	6.3
S-6g	Sand	*Chondrites*	B	47.16	50.14	50.08	5	4	147.5	6.3
S-6g	Sand	*Chondrites*	C	47.76	50.02	50.08	3	4	147.5	6.3

Table 1 (*Continued*).

Sand bed No.	Bed type	Nature of bed base	Site 1119 core	Base (mbsf)	Base (mcd)	Adopted (mcd)	Thickness (cm)	Adopted (cm)	Age (ka)	MIS
Zygochlamys			B	47.15	50.13	50.08	in S-6g		147.5	6.3
S-6h			B				in core gap			
S-6h	Sand	*Chondrites*	C	62.64	65.60	65.60	25	25	172.6	6.5
S-6i			B				in core gap			
S-6i	Sand	*Chondrites*	C	63.88	66.84	66.84	15	15	174.4	6.5
S-6j			B				in core gap			
S-6j	Sand	*Chondrites*	C	65.05	68.01	68.01	3		176.1	6.5
S-6k	Sand	*Chondrites*	B	64.65	69.95	69.95	17	17	178.9	6.6
S-6k			C				in core gap			
Zygochlamys			B	64.98	70.28	70.28			179.4	6.6
S-7a			B				in core gap			
S-7a	Shells		C	76.10	80.80	80.80	4	4	212.9	7.2
S-7b	Sand	*Chondrites*	B	76.51	82.52	82.59	65	68	223.9	7.4
S-7b	Sand	*Chondrites*	C	77.96	82.66	82.59	70	68	223.9	7.4
S-8a	Sand	*Chondrites*	B	79.03	85.04	84.99	20	18	240.6	7.5
S-8a	Sand	*Chondrites*	C	80.23	84.93	84.99	17	18	240.6	7.5
S-8b	Sand	*Chondrites*	B	80.45	86.46	86.33	100	105	250.0	8.2
S-8b	Sand	*Chondrites*	C	81.49	86.19	86.33	110	105	250.0	8.2
Intra-MIS 8 downlap unconformity (86.19 mcd, ~252–277 kybp)										
S-9a	Sand	*Chondrites*	C	86.81	92.75	92.75	5	5	335.7	9.3
S-9b	Sand	*Chondrites*	C	86.94	92.88	92.88	5	5	336.0	9.3
S-9c	Sand	*Chondrites*	C	87.06	93.00	93.00	5	5	336.3	9.3
S-10a	Sand	*Chondrites*	B	87.00	95.20	95.20	20	20	341.2	10.2
S-10b	Sand	*Chondrites*	B	87.13	95.33	95.33	10	10	341.5	10.2
S-10c	Sand	*Chondrites*	B	87.30	95.50	95.50	10	10	341.9	10.2

device that reacts samples with 100% orthophosphoric acid in a common acid bath. The gas generated passed through two water traps before being analysed by a duel-inlet Micromass Optima mass spectrometer. For calibration and accuracy, each analytical run of 40 samples included two international NBS19 standards ($\delta^{13}C_{PDB} = 1.95‰$; $\delta^{18}O_{PDB} = -2.2‰$), five internal bicarbonate standards, and five blanks. In addition, 10% of analyses were chosen as random duplicates to test reproducibility and comparability over different analytical runs. All duplicates agreed with the original analysis within 0.3‰, and the combined average of original plus duplicate was adopted for plotting.

3. Oceanographic setting

Site 1119 is located about 5 km seaward of the modern shelf edge which here lies at a depth of ~150 m (Fig. 2). The shelf watermass is driven northwards by prevailing southerly storms and by the ~2–50 cm/s Southland Current (Heath, 1972a, 1985; Carter and Heath, 1975; Chiswell, 1996; Orpin, 1997), the core of which comprises warm saline (>34.5‰) Subtropical Surface Water (STW; =Australasian surface water, ASW) which passes round the southern end of South Island from the Tasman Sea (Fig. 3). Most of the flow, which varies between 2–11 Sv (Heath, 1972a; Chiswell, 1996), is sourced from the southern branch of a cross-Tasman front at ~40°S (Heath, 1975; Stanton, 1973, 1976; Front A of Ridgway and Dunn, 2002, which is derived by eastward flow from the East Australian Current), with probably only a minor contribution from the weak zonal flow which occurs along the STF itself at ~45°S (Stanton and Ridgway, 1988; Sokolov and Rintoul, 1999). Shelf-parallel mean flows up to 28 cm/s are recorded for the Southland Current on the eastern South Island shelf, and bursts to 80 cm/s are known (Chiswell, 1996; Orpin, 1997). The presence of shelf-parallel sand ribbons and transverse dunes on the outer shelf seabed (Carter et al., 1985, fig. 18) suggests that augmentation of this motion to >100 cm/s occurs during storm events (cf. Carter and Herzer,

1979). The core of the Southland current today lies above the ~200–300 m isobaths, and a little further seawards the Southland Front separates the saline shelf water from the western edge of similarly north-travelling but cold Subantarctic Water (SAW) with a salinity of ~34.2‰ (Chiswell, 1996). The front is located about 80 km offshore, near the shelf edge, and its modern position is relatively stable through time (Chiswell, 1994). The outer parts of the Southland Current entrain some subantarctic water, through mixing across the STF (Heath, 1972a). This subantarctic influence is manifest in the occurrence of cold-water benthic molluscan assemblages on the outer shelf and upper slope of eastern South Island (Fleming, 1944; Powell, 1950; Dell, 1956). Both the Southland Front, and its STF continuation along the Chatham Rise, are today locked onto the bathymetry (Heath, 1972a, 1981), and palaeoceanographic studies suggest that, at least for the Chatham Rise, this locking has remained stable through recent glacial/interglacial (G/I) cycles (Fenner et al., 1992; Nelson et al., 1993; Weaver et al., 1998).

Seaward of the Southland Front, the oceanic Pacific waters are stratified into SAW (0–300 m), SAMW (300–800 m), AAIW (800–2000 m), and Circumpolar Deep Water (CDW; 2000–4500 m), the latter entrained within the Pacific deep western boundary current (e.g. Carter and McCave, 1997). SAMW and AAIW are both northward-flowing. Their range of densities corresponds to the location of the main thermocline, and they play an important role in ventilating the Pacific Southern Hemisphere subtropical gyre. Near Site 1119, these water masses travel as part of a cyclonic re-entrant in the regional flow, corresponding to the bathymetric influence of the Bounty Trough. In effect, SAMW–AAIW act as a clockwise contour current around the slopes of the Bounty Trough (Fig. 1; cf. Morris et al., 2001).

These water masses and their motions exert a controlling influence on sediment transport and deposition off eastern South Island. Today, Site 1119 is located just downslope of the core of the Southland Current, and near the top of the mid-slope belt of SAMW sediment drifts, though modern SAMW flow appears subdued (Fig. 3D). Fine-grained sediment is unmixed from the outer shelf during storms, and bypassed over the shelf edge to accumulate as an upper slope mud drape at depths below storm wave-base and Southland Current flow, and above the main SAMW–AAIW flow.

4. Stratigraphy and sedimentology

4.1. Changing palaeogeographies

4.1.1. Interglacial highstand

Site 1119, being located within the Canterbury Bight, penetrates the upper part of the eastern South Island passive margin sedimentary succession. The margin was created by rifting in the late Cretaceous, and has since experienced steadily decreasing rates of post-rift subsidence (Carter and Norris, 1976; Carter, 1988). The shelf edge and upper slope at the site are underlain by seaward-dipping reflectors which parallel the seafloor (Fig. 2), and which mark the seawards progradation of the outer shelf–upper slope seabed during the late Quaternary. Even at the high resolution of 3.5 kHz profiles, the dipping reflectors (palaeo-upper slopes) of MIS 6 appear to continue to the seafloor under the shelf edge. This indicates that little or no modern aggradation occurs of the surface of the outer shelf, where today only a very thin cover of <1 m thickness of reworked, biogenic-rich sediment accumulates. This is not surprising, given that the width of the mid-Canterbury shelf here is ~80 km, and that modern terrigenous sediment is confined to a northward-travelling shore-connected belt on the inner–middle shelf (Carter and Herzer, 1979). That the modern outer shelf seafloor sediments are shelly and sediment starved is well established (Andrews, 1973; Carter, 1975; Carter et al., 1985; Gray, 1993). Orpin et al. (1998) have described how these shell hashes spill over onto the upper slope, down to depths of several hundred metres, where they become intermixed with small amounts of Holocene mud. Thus during the Holocene interglacial highstand, Site 1119 has been located in relatively deep water (395 m), far offshore, and just downslope from a generally sediment-starved outer shelf.

4.1.2. Glacial lowstand

The geographic situation of Site 1119 during late Quaternary glacial lowstands was profoundly different. At an estimated depth of 130–135 m (Carter et al., 1986; Browne and Naish, 2003), the MIS 2 shoreline was located near the shelf–slope break, and only ~15 km inboard of Site 1119. Sediment from the New Zealand Southern Alps was delivered directly to this shoreline by east coast rivers (Griffiths and Glasby, 1985; the modern flux being ~41 Mt/yr). Copious micaceous, glaciogenic mud settled out of nearshore suspension along deltaic foresets (Carter et al., 1985, fig. 15c), which prograded across the narrow shelf and merged onto the nearby upper slope. In keeping with this, a seaward-dipping zone of amalgamated seismic reflectors (sand-rich), which underlie the outer shelf just inboard of Site 1119, pass seawards into discrete reflectors (thin sands) separated by thicker, acoustically transparent intervals (muds) (Fig. 2); further seawards, the sand reflectors fade out altogether. Such a pattern is consistent with nearshore prodelta sands passing offshore – and, in this instance, downslope – into distal muds (cf. Browne and Naish, 2003). Thus during recent glacial lowstands, Site 1119 was located in relatively shallow water (~250 m) within the distal part of the shore-connected sedimentary prism, and well within the coastal zone of rapid terrigenous sedimentation.

4.2. Assignment of time scale (0–100 mcd)

The interpretation of Site 1119 stratigraphy (Fig. 4) is aided by the presence of a G/I lithological cyclicity which stems from the changing palaeogeographies just described, and by the availability for comparative purposes of: (1) nearby high resolution oxygen isotope curves from DSDP Site 594 (Nelson et al., 1986, 1993), and ODP Site 1123 (Hall et al., 2001); and (2) the ~375+ kyr-long south polar climate record from the Vostok drillsite (Petit et al., 1999). Interpretation is hindered, on the other hand, by the shallow water location of the site, which has caused the development of minor diastems at the base of at least some interglacial sand beds and which also, through helping to control G/I fluctuations in the position of the STF, has affected the detailed pattern of the stable isotope measurements.

There is a striking overall similarity between the Vostok deuterium record (Petit et al., 1999), which reflects atmospheric temperature change on the Antarctic plateau, and the Site 1119 γ-ray curve, which reflects the waxing and waning of the South Island mountain ice-cap. A time scale has therefore been assigned to the MIS 5.5 and older parts of the 1119 core (42.78–100 mcd) by matching 15 distinctive features on the γ-ray curve to their counterparts within the Vostok climatic record, as tuned and dated by Shackleton (2000), using linear interpolation to derive ages between each pair of control points (Fig. 5; Table 2). Age control over the top 18.67 mcd of the core is provided by six AMS radiocarbon dates, which have been converted to calendar years using the CALPAL correction programme (Joris and Weninger, 2000; CALPAL, 2003) (Table 3). The lab-

Fig. 4. (see overleaf) Core-depth plot for four oceanographic proxy parameters through the upper 100 mcd for Site 1119. Position of sands, shellbeds and *Zygochlamys* indicated on the summary stratigraphic log at the base of the figure, with key below. Anomalies MIA 1–7 in the oxygen isotope record, anomalies Ga 1–4 and Gb 1–2 in the γ-ray record, and sands/shellbeds S1–S10 on the graphic core log are indicated by appropriate lettering. Sands/shellbeds are numbered and lettered according to their order of occurrence within marine isotope stages (MIS) 1–10, with the individual lettered beds shown above the log. Direct measurements of carbonate content are plotted on the colour reflectance (proxy carbonate) record as discrete points.

Fig. 5. (see overleaf) Stratigraphy of the upper 100 mcd for Site 1119 plotted against a time scale derived from AMS radiocarbon dates (last 39 ka) and by comparison between the oceanographic proxy records and the Vostok ice core (Petit et al., 1999; Shackleton, 2000). Position of time scale control points indicated by black triangles along the base of the γ-ray record (see also Table 2). See text for a detailed discussion of the derivation of the time scale. Inset (top left of γ-ray record): proxy climate record for the last 30 kyr for South Island, New Zealand, as indicated by oxygen isotope measurements on speleothems from Nelson (Hellstrom et al., 1998).

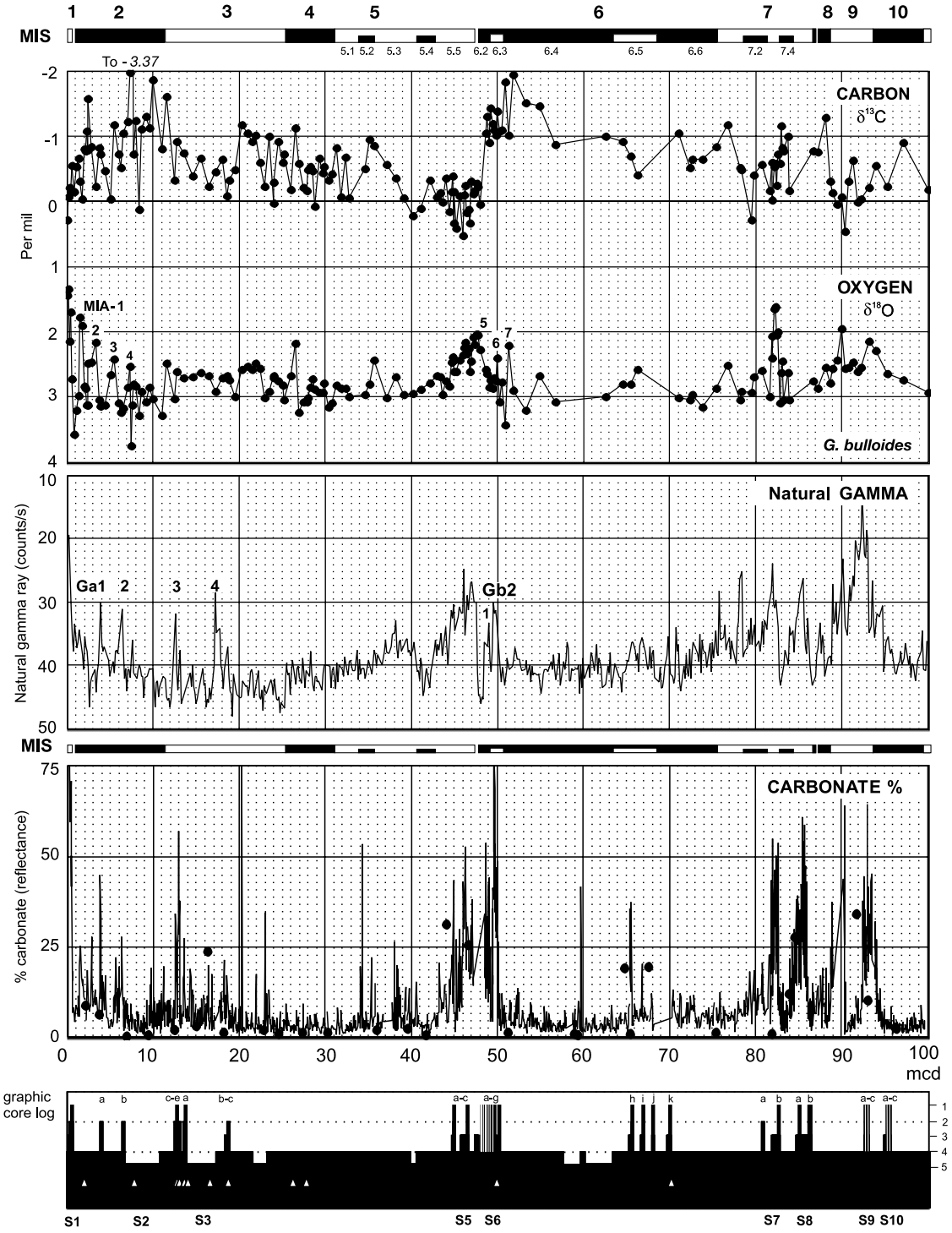

1. Sharp, *Chondrites*-burrowed base 2. Shell layer 3. Sand bed 4. Massive mud
5. Cm-banded muds Triangle. *Zygochlamys delicatula*

Fig. 4.

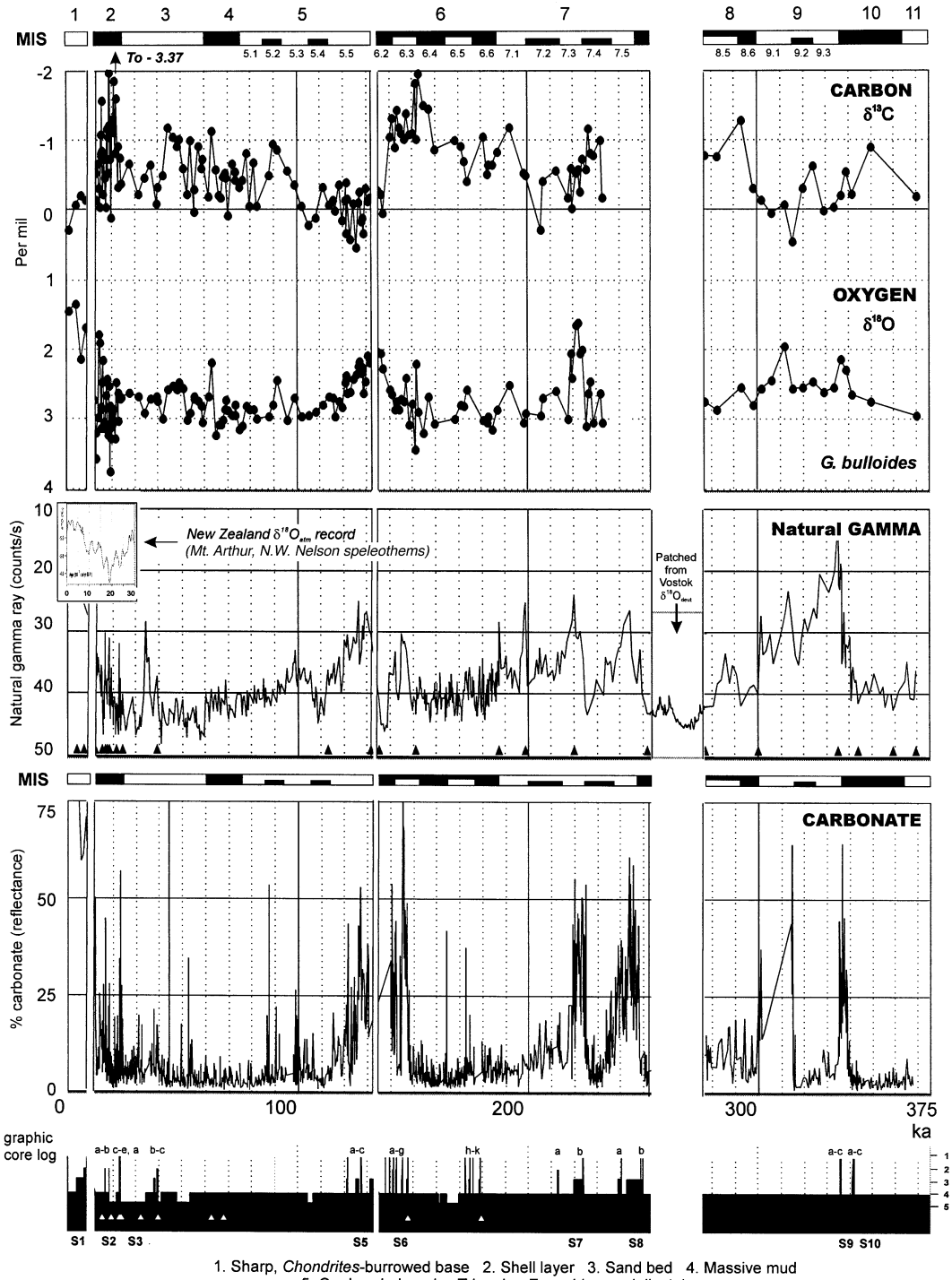
MIS
To - 3.37
CARBON
δ13C
OXYGEN
δ18O
G. bulloides
Per mil
New Zealand δ18Oatm record
(Mt. Arthur, N.W. Nelson speleothems)
Natural GAMMA
Patched from Vostok δ18Oatm
Natural gamma ray (counts/s)
CARBONATE
% carbonate (reflectance)
ka
graphic core log
S1 S2 S3 S5 S6 S7 S8 S9 S10
1. Sharp, Chondrites-burrowed base 2. Shell layer 3. Sand bed 4. Massive mud
5. Cm-banded muds Triangle. Zygochlamys delicatula

Fig. 5.

Table 2
Table of control points and sedimentation rates for the Site 1119 age model

mcd	Control (cal ^{14}C ka)	Age model	Sedimentation rate (cm/kyr)	Correlation
0.00	seabed	0	5	Assumed
0.45	estimate	9000	Diastem	Estimate after Herzer (1981)
0.46	estimate	11975	55	Estimate on sedimentation rate between 0.46 and 0.60 mcd
0.60	(12230)	12230	55	Individual AMS date
2.07	(15210)	15157	141	Fitted AMS date
3.84	(16840)	16419	141	Fitted AMS date
5.04	(16820)	17278	141	Fitted AMS date
6.31	(17410)	18180	141	Fitted AMS date
11.04	(22720)	21531	141	Fitted AMS date
14.59	(23430)	24059	27	Fitted AMS date
18.67	(39330)	39330	33	Individual AMS date
42.78	Vostok	113000	25	MIS 5.1–4 boundary
47.58	Vostok	132000	Diastem	Near base of MIS 5.5
47.59	Vostok	135000	20	Assumed MIS 6–5 diastem of 3 ky
50.78	Vostok	151000	69	Near 6.4–6.3 boundary
75.82	Vostok	187500	22	MIS 7–6 boundary
78.37	Vostok	199000	17	MIS 7.1 peak
82.03	Vostok	220000	14	MIS 7.3 peak
86.62	Vostok	252000	Unconformity	In top of MIS 8.2
86.63	Vostok	277000	10	MIS 8.5–8.4 boundary
88.82	Vostok	300000	10	MIS 9–8 boundary
92.42	Vostok	335000	45	MIS 9.3 peak
96.43	Vostok	344000	14	Top MIS-10.2
98.57	Vostok	359500	14	MIS 10.4 centre
100.10	Vostok	370000		Top of MIS 11

The model is based upon radiocarbon age control down to ~39 ka (18.67 mcd), and prior to that by matching individualistic features of the climatic record between the 1119 onboard MST natural γ radiation curve (a proxy for mud delivery to the site) and the deuterium record from the Vostok ice core (a proxy for Antarctic air temperature; Petit et al., 1999), using the Vostok time scale tuned to insolation at 65°N by Shackleton (2000). To reduce arbitrary changes in sedimentation rate, a linear age model was fitted to the six AMS dates between 2.07 and 14.95 (age = 13 700+710*mcd; $R^2 = 0.96$). Because of the marine reservoir correction uncertainties, the radiocarbon-controlled part of the age model is provisional. Age errors up to ±1 kyr are possible back to ~25 ka, and up to ±3 kyr between 25 and 40 ka.

Table 3
Accelerator mass spectrometry radiocarbon dates from Site 1119

Core mbsf	mcd	ANSTO No.	Sample material	^{14}C age (conventional)	Error	Reservoir correction	Corrected age	Calibrated age BP	Error
B-0.56	0.60	OZG099	serpulids	13010	80	−800	12210	12230	290
B-2.03	2.07	OZG516	serpulids	15640	70	−1200	14440	15210	230
B-3.80	3.84	OZG0100	serpulids	17420	90	−1200	16220	16840	250
B-4.80	5.04	OZG517	serpulids	17400	70	−1200	16200	16820	240
C-6.15	6.31	OZG515	*Tawera*	18630	90	−1980	16650	17410	300
B-10.08	11.04	OZG0102	serpulids	23150	140	−1980	21170	22720	280
B-14.35	14.59	OZG518	serpulids	23890	210	−1980	21910	23430	270
B-17.43	18.67	OZG513	*Tawera*	38500	500	−1200	37300	39330	190

Laboratory determinations were provided by the Australian Nuclear Science and Technology Organisation. Dates were corrected for marine reservoir age after the data provided by Sikes et al. (2000), and converted to calendar year estimates using CALPAL (CALPAL, 2003) and the INTCAL98 age model (Stuiver et al., 1998).

oratory error for the AMS dates ranges between 70 and 500 years, but the uncertainty of marine reservoir corrections for dates older than ~12 ka adds another, and mostly much larger, source of error. We have used the best reservoir corrections available for the Southwest Pacific (Sikes et al., 2000), but even so our estimated time scale since 40 ka may be in error by up to ~1–2 kyr. The greatest uncertainty in our overall time scale model comes in the MIS 3–5.3 interval, between the lowest AMS radiocarbon date (18.67 mcd, 39.3 cal ka) and the sharp step decrease in γ-ray value which we correlate with the end of MIS 5.5 in the Vostok core (42.78 mcd, 113 ka). Though some peaks and troughs might be matched between them, the 1119 γ-ray curve and the Vostok record differ in detail over the MIS 3–5.3 interval. Therefore, and in the absence of additional specific age indicators, we have preferred to leave the age model for this section of the core 'floating' between the 39.3 ka and 113 ka tie-points.

The resulting time scale model (Fig. 5) shows that the upper 100 mcd of Site 1119 represents an almost continuous section through MIS 1–11, apart from probably two short basal interglacial diastems and a ~25-kyr-long, intra-MIS 8, downlap unconformity at 86.19 mcd (Fig. 5). By analogy with the definite occurrence of a ~3-kyr-long diastem at the base of the Holocene interglacial sand (S-1), we have inserted into our model a similar diastem below the basal MIS 5 sand (S-5c; Fig. 4). We infer that the MIS 5.5.3 peak and a small amount of latest MIS 6 are here missing, across an estimated ~132–135 ka gap (Fig. 6).

4.3. Sedimentary facies

In keeping with a changing G/I setting, Site

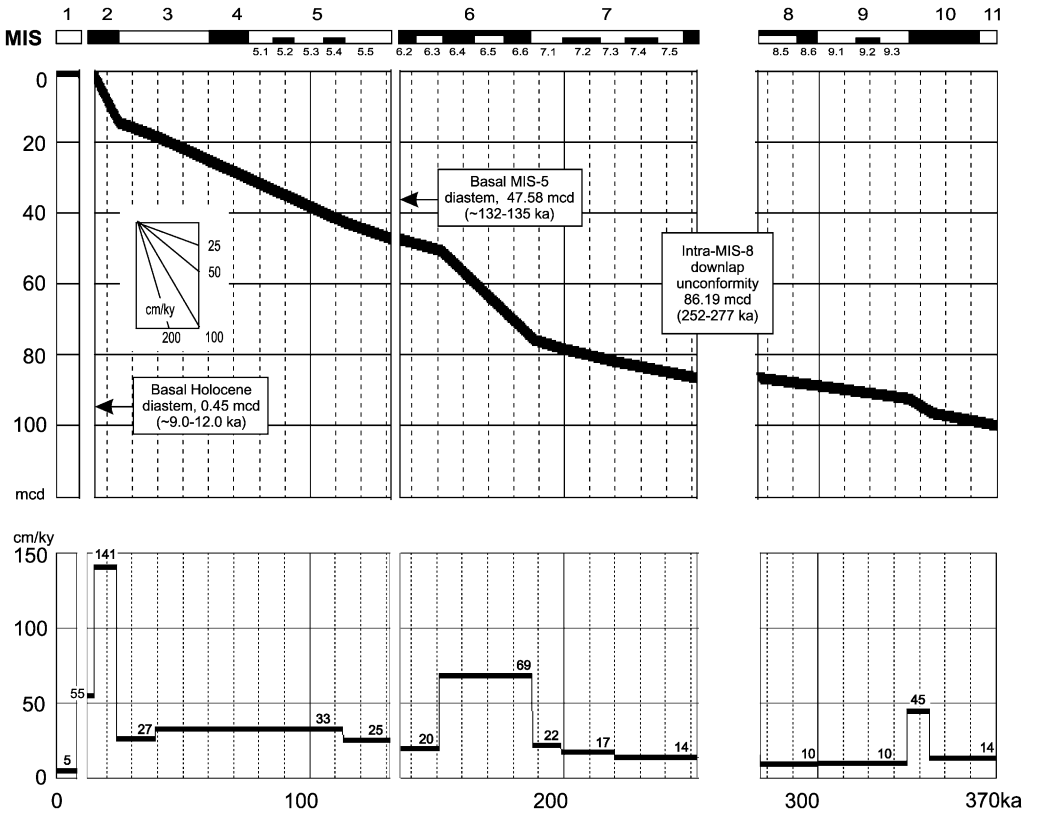

Fig. 6. Time–depth curve (upper) and estimated sedimentation rates (lower) for the upper 100 mcd of Site 1119 plotted against the age model of Table 2.

1119 penetrated a 495-m-thick cyclic succession of grey mudstone, mostly silty clay, punctuated by intervals containing 3–65-cm-thick, irregularly spaced, graded beds of olive grey, sharp-based (*Chondrites*-burrowed), shelly (*Tawera spissa*), terrigenous fine sand (mode ~150 μm) to mud (Table 1; Fig. 4). Thicker sand units (10–105 cm thick) are concentrated within the relatively warm-climate intervals MIS 1, 5.5 and 7. The intervening grey silty clays which represent cold-climate stages MIS 2–4, 6, 8 and 10 have low organic carbon content (average 0.34%), low but variable carbonate content (generally < 5%), enhanced siliceous and impoverished calcareous microfaunas, and the spasmodic occurrence of the cold water scallop *Zygochlamys delicatula*. They also occasionally contain thin (usually 2–10 cm thick) shelly sands which, for MIS 2 at least, are rich in bryozoa and serpulids.

At the top of the 1119 core, the MIS 1 (Holocene) interglacial interval corresponds to a 45-cm-thick, sharp-based, *Chondrites*-burrowed unit of olive grey shelly sand grading up to sandy mud, and resting sharply on massive, buttery mud. The oxygen isotope ratios of ~1.5‰ measured through the graded sand-mud bed (Fig. 5) are the lightest which occur at Site 1119, and are comparable to the Holocene planktic foraminiferal ratios measured nearby at DSDP 594 (~1.5‰; Nelson et al., 1993). A similar change from underlying grey 'glacial' silty clay to sharp-based, brownish, Holocene shelly sand and muddy sand is widespread in piston cores from the eastern South Island outer shelf and upper slope. The youngest sediments below the change have a latest Pleistocene age of ~12 ^{14}C ka (Griggs et al., 1983; and Table 3 herein), whereas the oldest known dates from above are 8.6–9.4 ^{14}C ka (Herzer, 1981; = 8.5–9.5 cal ^{14}C ka). Therefore, a small amount of time, probably varying from place to place but generally not longer than a few thousand years, is missing across the sharp, burrowed base to the Holocene sand veneer. By analogy, similar small diastems may occur at the bases of the older basal interglacial sands which occur deeper in the succession.

Below the Holocene sand–mud (0–0.45 mcd), MIS 2 (0.45–11.04 mcd) contains in its lower part a 4-m-thick interval of interbedded, sharp-based, lighter- and darker-grey clay beds up to 3 cm in individual thickness (Fig. 4, sediment log). Similar unbioturbated, cm-scale banded, darker and lighter-coloured clays are also present within MIS 3–4 (14–17 mcd, 21.0–23.5 mcd) and MIS 6 (57.0–63.0 mcd). At ODP 893A, in the Santa Barbara basin, Kennett and Ingram (1995) interpreted similarly layered, though more finely laminated, muds as representing periods of anoxia which suppressed the epibenthos, and hence precluded bioturbation. In contrast, the banded muds at Site 1119 mark rapid, individual sedimentation pulses such as river flood events, and the well ventilated nature of the site means that oceanographic (as opposed to burial) anoxia is unlikely.

It is important to note that the graded sand–mud rhythms which are characteristic of both interglacial and peak glacial intervals at Site 1119 show no Bouma features, nor indeed any conspicuous sedimentary structures. Rather, apart from upward grainsize diminution, which may be repeated more than once within a bed, the beds are structureless and have the appearance of tractionites rather than turbidites. The immediate source of their constituent terrigenous sand is unclear. Its low-grade metamorphic provenance is similar to that of modern seabed sands and gravels from across the shelf (Herzer, 1981), and indicates an ultimate derivation from the basement greywackes and schists of eastern South Island. However, no highstand cross-shelf sand transport route exists on the modern shelf. This fact, and their well-sorted nature and very fine to fine sand grainsize, suggests that the 1119 sands are of multicyclic (relict) origin. We infer that during times of enhanced bottom current activity on the outer shelf and upper slope, which occurred invariably during interglacials, but also during some peak glacials, these sands were reworked downslope and alongslope from littoral sand bodies which were first deposited near the outer edge of the shelf during preceding glacial lowstands.

4.4. Sedimentation rates

On the Site 1119 age-depth curve (Fig. 6), the

intra MIS-8 downlap unconformity at 86.19 mcd (252–277 ka) separates the succession into a part above with an average sedimentation rate of 34 cm/kyr (upper slope foresets), and a part below with a lower average rate of 14 cm/kyr (mid-slope sediment drifts). The precise position at which other graphical (and therefore sedimentation rate) changes occur on Fig. 6 is, of course, an accidental result of the positions of time scale correlation points or determinations. Nonetheless, the following comments are warranted:

- peak interglacial intervals MIS 1, 5, 7 and 9 are characterised by low sedimentation rates of 5–25 cm/kyr, whereas intermediate sedimentation rates of 33–69 cm/kyr characterise I/G transitions and early glacials;
- glacial MIS 6 displays its highest sedimentation rate of 69 cm/kyr during the early glacial maximum, reducing to 20 cm/kyr during the late glacial maximum;
- there is an upward increase in the maximum glacial sedimentation rate from MIS 10 (45 cm/kyr) to MIS 6 (69 cm/kyr) to MIS 2 (141 cm/kyr), in keeping with progressively shallowing water over this period due to sediment accretion and therefore perhaps reflecting the proximity of the site to the nearby shoreline sediment source;
- in analogous fashion, the higher average sedimentation rates above the intra-MIS 8 unconformity reflect the deposition of the sediments there as deltaic foresets near to the shoreline source, in contrast to the more slowly deposited and deeper-water drift sediments (MIS 8–11) below.

4.5. Extent of the downlap unconformity

Having determined the time scale and sedimentation rates across the 1119 core, we are able to estimate the period of time and thickness of sediment which is missing across the downlap unconformity at ~86.19 mcd. In the core, the base of sand unit S-8b separates latest MIS 8 above from MIS 8.5 and older sediments below. The estimated gap is 25 kyr, between ~252 and ~277 ka (Fig. 5). That sand S-8b, at 105 cm thick and containing composite internal grading, is the thickest in the MIS 1–8 succession might result from its being located just above the unconformity. Applying the sedimentation rate which characterises MIS 8.5–10 just below the unconformity, we estimate that a minimum of ~2.50 m of sediment is missing from the section. The real amount missing could, however, attain twice this figure or more if sedimentation rates increased during the MIS 8.4–8.2 glaciation, as they undoubtedly did during MIS 6 and MIS 2. The missing few metres of sediment, whatever its precise thickness, was doubtless removed by a similar (but slightly stronger) current to that which effected deposition of the thick S-8b sand.

4.6. Frontal stability or migrations?

Recent work on the history of the STF in the Southwest Pacific has concentrated on the Chatham Rise sector of the front, and writers have provided strong arguments that there the front remained 'locked' to the bathymetric crest of the Rise throughout the G/I cycle (Fenner et al., 1992; Nelson et al., 1993; Weaver et al., 1998; Carter et al., 2000). We might infer, therefore, that the Southland Front similarly remained 'locked' to the eastern South Island shelf edge during glaciations. Instead, the lithological cyclicity and the characteristic presence of sandier (higher energy) sediments in interglacial core intervals at Site 1119 suggests that migrations of the STF have occurred across the site. Whether and how such changes occurred depends upon the G/I behaviour of zonal flow across the Tasman Sea (cf. Fig. 1), because today the Southland Current and its accompanying front are derived from the portion of the trans-Tasman STW flow that is diverted into a loop south of South Island. This diversion is caused by the presence of the Challenger Plateau, which is located where the mid-Tasman eastward flow derived from the East Australian Current impinges upon the shoaling New Zealand bathymetry, causing a north/south bifurcation of the flow at ~43°S. The ~130 m drop in sea level and northward frontal movement which occurred during recent glaciations could on each occasion have changed the interaction between Tasman zonal flow and the Challenger Plateau, such that the entire glacial flow turned

north as a single eastern Tasman boundary current. This would have diverted the STF north of South Island, cut off the Southland Current, and left the narrow east coast shelf to be bathed completely in cold subantarctic waters (cf. Weaver et al., 1997, 1998).

Considering such possibilities in the context of Site 1119, the three major alternatives are that during glaciations the Southland Front (=STF) might have been: (1) located seaward of its modern position, and of Site 1119, above deeper, mid-slope water; or (2) located in, or even landwards of, its modern position along the shelf edge; or (3) diverted entirely around the west of South Island, via an enhanced East Auckland current, leaving the eastern shelf to be occupied by colder SAW. Significant oceanographic difficulties accompany the second and third of these interpretations. Regarding (2), at last glacial lowstand the eastern South Island shelf was generally not more than 15 km wide and had a depth of ~20 m at the shelf break. Thus only very small volumes of STW flow would have been possible inboard of a front located at or landwards of the shelf edge. Regarding (3), the bathymetry of the Challenger Plateau region has a similar shape regardless of whether sea level is located at its modern position or at −130 m depth. Therefore, no particular reason exists as to why the trans-Tasman flow should be diverted entirely to the north throughout glacial lowstands. These considerations lead us to favour the first interpretation for G/I frontal movements, i.e. that as the climate cooled, and sea level fell, the Southland Front moved eastward across Site 1119 to occupy a position seawards of the site during glaciations. In Section 5, we examine the available palaeoceanographic proxy data for Site 1119 to test this hypothesis.

5. Palaeoceanography

Because of the light that it throws on migrations of the STF, we discuss the $\delta^{13}C$ record for Site 1119 first, after which we consider in turn the $\delta^{18}O$, natural γ-ray and reflectance (% carbonate) records.

5.1. Planktic $\delta^{13}C$ record

For the two major G/I cycles since MIS 7, the change from heavy interglacial to light glacial $\delta^{13}C$ which takes place at Site 1119 appears to take place gradually, whereas the converse change from light (cold) to heavy (warm) is abrupt (Figs. 4 and 5), i.e. the carbon isotope curve exhibits a classic 'termination' pattern similar to that first commented on for the oxygen isotope curve by Broecker and van Donk (1970). $\delta^{13}C$ oscillations of ~1‰ with a frequency of several thousand years are superimposed on this first order rhythmicity. In addition, smaller high-frequency $\delta^{13}C$ oscillations as short as ~1 kyr occur during MIS 2 and 6, where they are accompanied by similar fluctuations in the oxygen isotope record.

Changes in carbon isotope values are often interpreted as reflecting water mass nutrient content. A high rate of air-sea carbon isotopic exchange makes any such linkage weak in cold, southern waters, where, because different water masses exhibit characteristic $\delta^{13}C$ values, $\delta^{13}C$ is instead a valuable tool for tracing water mass histories (Charles and Fairbanks, 1992; Lynch-Stieglitz and Fairbanks, 1994; Charles et al., 1996). In the Southwest Pacific, the major water masses are characterised by the following values (Nelson et al., 1993, 2000):

	Modern $\delta^{13}C$‰	Last glacial $\delta^{13}C$‰
STW	−0.8 to −1.2	
SAW	0.5 to −0.5	0.5 to −0.5
SAMW–AAIW	0.5 to 0.0	−0.5 to −0.8
CDW	0.4 to 0.0	−1.0 to −1.5

Applying this knowledge to the $\delta^{13}C$ record at Site 1119 (Figs. 4 and 5), and as a refinement of the G/I-scale saw-toothed termination pattern, three broad $\delta^{13}C$ bands can be identified each of which corresponds to the isotope ratio typical of a particular watermass (Fig. 7). It is thereby apparent that the surface waters above Site 1119 came under the successive influence of three distinctly different water masses during G/I cycles. During interglacials MIS 1 and 5.5, and also briefly during stadials MIS 7.2 and 9.2, the site was bathed in SAW ($\delta^{13}C$, 0–0.5‰); during intermediate cli-

matic periods MIS 3–5.3, MIS 6.3–6.6, MIS 7.3–7.4 and MIS 9.3, SAW was replaced by a mixed STW–SAW water mass ($\delta^{13}C$, 0 to −1.0‰); and during peak cold glaciations MIS 2 and MIS 6.2–6.3 the ambient water mass possessed very light $\delta^{13}C$ values of −1.0 to −2.0‰ or less, probably reflecting the presence of upwelled CDW (cf. Nelson et al., 2000; Mackensen et al., 2001). Strongly negative values may also represent increased productivity (e.g. Kowalski and Meyers, 1997; Matsumoto and Lynch-Stieglitz, 1999) and/or an increased ratio of foraminifera:nannofossils (Dudley and Nelson, 1989). Within each of these $\delta^{13}C$ bands, higher frequency fluctuations of 0.5–1.0‰ occur on a time scale of 1–5 kyr. We interpret these fluctuations as marking the mixing of the STW and SAW water masses across the STF zone, as indeed occurs commonly today (Heath, 1975). Some of the fluctuations may also represent lesser movements in the position of the STF.

The individual periods of SAW and STW $\delta^{13}C$ water mass bands at Site 1119 are separated from each other by rapid and mostly unidirectional swings in $\delta^{13}C$ value of 1.0–1.5‰ magnitude, each example of which represents the passage over the site of the STF. These features are labelled S (frontal passage *Seaward*) 1–3 and L (frontal passage *Landward*) 2–3 on Fig. 7. Passage L1, which must have occurred across the MIS 8–7 boundary, is not represented in the data and is inferred to lie mostly within the downlap unconformity. Passage L3 was a complex, multi-stage event which comprised an initial landward passage (L3a), followed by seaward retreat, landward advance (L3b), early Holocene stasis, and then a final landward movement (L3c) (upper inset, Fig. 7). These data suggest that the STF only reached

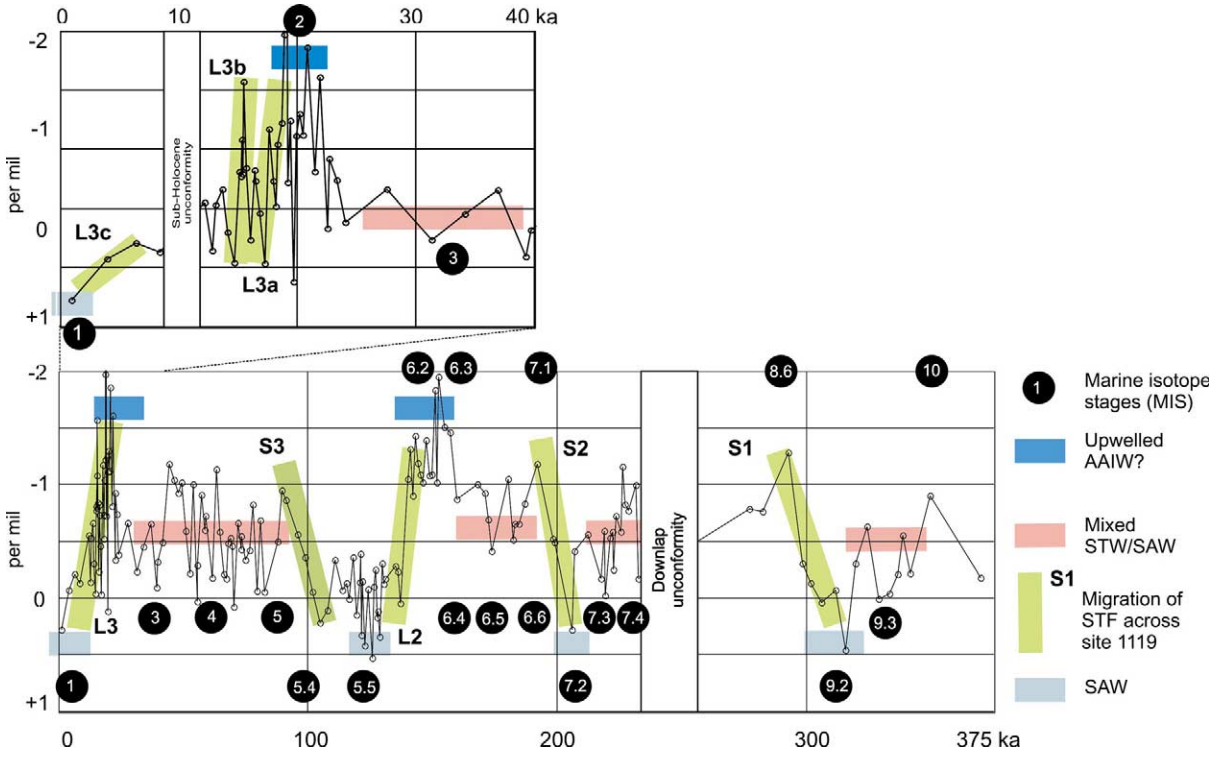

Fig. 7. Annotated carbon isotope record for Site 1119, depicting the changing water masses present through time (horizontal coloured bars) and the seaward (S1–S3) and landward (L1–2) migrations of the Subtropical Front (STF) across the site. Marine isotope stages (MIS) indicated by white numbers within black circles. Inset (top left): expanded record for the last 40 ka, showing the presence of three phases of landward movement (L3a–3c) of the STF during and after the peak of the last glaciation. See text for detailed explanation.

its modern position, inboard of Site 1119, in about the mid-Holocene. More generally, pulses of seaward (I/G) frontal migration across the site lasted ~10 kyr, whereas landward (G/I) migration was more rapid and for L3a, 3b, 3c and 2 took place in ~5 kyr or less. Lastly, the short periods of very negative $\delta^{13}C$ values at the peaks of MIS 2 and MIS 6.2–6.3, which are inferred to mark AAIW and perhaps CDW influence, start and finish rapidly over periods as short as ~1–3 kyr.

The three seaward frontal passages all commenced shortly after the climatic optimum of their corresponding interglacial periods, during MIS 9.2, 7.2 and 5.4, respectively. Perhaps surprisingly, and as discussed more fully later in this paper, landward frontal passages L2 and L3 occurred at the very end of the MIS 6.2 and 2.2 peak cold periods, entirely (L2) or mostly (L3) prior to their respective G/I boundaries (Fig. 7).

The frontal behaviour just discussed is most apparent in the $\delta^{13}C$ record (Fig. 7). In contrast, no particular signature appears to mark the STF migrations in the reflectance or γ-ray records (Fig. 5). However, the end of frontal passages S1, S2 and S3 are all marked by small $\delta^{18}O$ depletions. Therefore, the frontal migrations do not just control the nature of the carbon isotope record but probably cause also some of the conspicuous variability of the oxygen isotope record. Though the overall picture is clear, the complexity of watermass mixture, changing ocean chemistry and changing temperature which accompanied the frontal migrations through Site 1119 is such that not every detail of the record is necessarily interpretable.

5.1.1. Implications of glacial/interglacial frontal migration

The frontal movements that we have just inferred are counter-intuitive, in two separate ways. First, we normally expect the STF to move northwards (or, for the Southland Front sector, northwestwards) during an I/G transition (e.g. Howard and Prell, 1992; Wells and Connell, 1997), whereas, in the vicinity of Site 1119 bathymetric and sea-level steering in fact forces the front to move southeastwards. Second, where watermass properties are concerned, we generally expect a colder water mass to replace a warmer water mass during glaciations; in fact, because of the bathymetric forcing of the STF in a seawards direction, at Site 1119 a warmer STW water mass replaces the colder SAW during glacial periods. These water mass migrations notwithstanding, the overall cooling that both water masses experience during a glaciation may still result in a deglacial temperature rise at a particular site. Marine analogue techique (MAT) foraminiferal analyses (Wilson et al., 2002; Wilson, pers. commun.) indicate that a sea surface temperature (SST) G/I warming of ~3–4°C occurred at Site 1119 during recent deglaciations. That this is only about one-half of the G/I warming recorded at nearby Site 594 (Nelson et al., 1993) reflects the strong moderating influence of water mass substitution at Site 1119.

5.2. Planktic $\delta^{18}O$ record

The character of the Site 1119 oxygen isotope curve shows enough correspondence to the generalised SPECMAP curve (Imbrie et al., 1984) to allow the identification of the major climatic cycles present (Figs. 4 and 5). The curve is broadly similar also to the regionally important DSDP 594 (Nelson et al., 1993) and Vostok deuterium (Petit et al., 1999) records. Unusually, however, the 1119 $\delta^{18}O$ curve departs from the normal 'saw-toothed' pattern and instead displays a catenary shape. At the same time, the detail of the $\delta^{18}O$ curve is subdued, and also departs significantly from standard records.

5.2.1. Subdivisions of MIS 5

The base of MIS 5.5 is unambiguously demarcated at 47.58 mcd by the light $\delta^{18}O$ value of 1.92‰ in the base of graded sand bed 5c (Figs. 4 and 5), where sharp reflectance (high), γ-ray (low) and foraminiferal (low percentage of sinistral *Neogloboquadrina pachyderma*, high SST; Wilson et al., 2002 and pers. commun.) changes also occur. Above this level, a bilobed MIS 5.5 peak is evident, above which again $\delta^{18}O$ values increase progressively to values (at and above ~40 mcd) which fluctuate around 2.5–3.0‰

without obvious substage demarcations. Over the same interval, the γ-ray curve clearly demarcates MIS 5.3–5.5. The change from the higher MIS 5.5 isotope values to the MIS 5.1–early 5.5 'background' level is completed at 39 mcd (~100 ka), near the middle of MIS 5.3. This change corresponds to the S3 movement of the STF inferred from $\delta^{13}C$ data (Fig. 7), which caused the disappearance from Site 1119 of the SAW water mass from which the MIS 5.5 sediments were deposited. Throughout substages 5.1–5.3, once sea level had fallen from its early 5.5 peak by only about 30 m (compare Fig. 4 with, e.g. Cutler et al., 2003, fig. 7), and continuing through MIS 3–4, intermediate $\delta^{18}O$ values are consistent with Site 1119 planktic forams inhabiting an STW or mixed STW/SAW water mass (see discussion under carbon isotopes, above).

5.2.2. MIS 2 oscillations

The interval between the strongly positive oxygen isotope value of 3.75‰ at 7.54 mcd (~19.2 ka) and the base-Holocene diastem at 0.45 mcd (~12.9 ka) is interrupted by four substantial, short $\delta^{18}O$ oscillations. These oscillations have successively more negative peaks at 7.34 mcd (18.9 ka), 5.54 mcd (~17.6 ka), 3.34 mcd (~16.1 ka), and 1.56 mcd (~14.1 ka), which we term marine isotope anomalies (MIA) 4–1, respectively; three similar peaks in MIS 6 are assigned to MIA 5–7 (Table 4; Figs. 4 and 5). These light oxygen peaks are not matched consistently by any features in the $\delta^{13}C$, γ-ray or colour reflectance records. Neither do the oscillations correspond simply with any established standard climatic record, though similar fluctuations which occur after the LGM elsewhere have been attributed to meltwater pulses (e.g. Kennett and Shackleton, 1975; Flower and Kennett, 1995; Clark et al., 1996), or to Younger Dryas-style oscillations in the North Atlantic thermohaline circulation (e.g. Sarnthein and Tiedemann, 1990). The MIA 1, 2 and 3 fluctuations post-date the estimated 19.2 ka LGM at Site 1119, and therefore could represent meltwater pulses. The first major post-LGM meltwater pulse in the Northern Hemisphere has been assigned an age of ~13.8 ka (Clark et al., 1996; Bard et al., 1996), which corresponds within error to our estimate of the age of MIA 1. It is possible too that MIA 2–3 represent earlier Southern Hemisphere meltwater episodes. Alternatively, and perhaps more likely, these isotope excursions may represent variations in the position or intensity of the STF as it migrated landwards across Site 1119, with each $\delta^{18}O$ enrichment-depletion oscillation marking the encroachment and retreat of isotopically-positive (cold) SAW. In this regard, we note that such oscillations occur exclusively within cold periods of the MIS 2 and 6.2–6.3 glaciations (Fig. 5).

5.2.3. Amplitude of $\delta^{18}O$ signal during climatic cycling

Except during the Holocene where corrected $\delta^{18}O$ values are as light as 1.6‰, interglacial $\delta^{18}O$ values at Site 1119 consistently lie between 2.3 and 2.5‰, i.e. the amplitude of the MIS 2–1 G/I change is significantly larger than earlier G/I changes. The reason for this is not fully understood, but it may result from a combination of: (1) the structure of the Site 1119 isotope curve being controlled largely by G/I changing of surface water masses caused by migrations of the STF; and (2) that it is only during the most recent (Holocene) interglacial, perhaps due to water mass displacements caused by progressive seabed shoaling, that surface waters at Site 1119 were situated close enough to the highstand position of the STF for them to be affected by pulses of warmer STW intermixing seawards across the front.

5.2.4. Summary

We conclude that the subdued $\delta^{18}O$ record for Site 1119 (Figs. 4 and 5) reflects the compromise signal which results from competition throughout a G/I cycle between the negative $\delta^{18}O$ forcing tendency of global-ocean reservoir change and positive variations in $\delta^{18}O$ imposed by the local migration of the STF. The migrations result in the presence of SAW at the site during interglacials, STW during colder periods, and water with some AAIW or CDW characteristics during peak glaciations. The catenary shape of the 1119 $\delta^{18}O$ record is thus a local rather than a global feature,

Table 4
Table of oxygen and carbon isotope values measured for the top 100 mcd of Site 1119

Sample No.	Core	mbsf	mcd	Age model	$\delta^{13}C$	$\delta^{18}O$
1368585	B	0.01	0.05	1000	0.28	1.44
1368587	B	0.17	0.2	4000	−0.07	1.35
1368591	B	0.28	0.32	6400	−0.21	2.14
1453462	B	0.38	0.42	8400	−0.13	1.69
1453470	B	0.56	0.6	12230	−0.55	2.72
1368593	B	0.86	0.9	12827	−0.14	3.57
1453472	B	1.02	1.06	13146	−0.53	3.2
1453474	B	1.3	1.34	13703	−0.66	2.98
1454723	B	1.52	1.56	14141	−0.3	1.78
1454725	B	1.8	1.84	14699	−0.04	1.91
1511272	B	2.03	2.07	15157	−0.81	2.83
1511273	B	2.15	2.19	15255	−0.77	2.87
1454727	B	2.3	2.34	15361	−1.08	3.13
1511274	B	2.38	2.42	15418	−0.79	3.13
1481040	B	2.44	2.48	15461	−1.57	2.48
1454729	B	2.8	2.84	15716	−0.84	2.47
1453477	B	3.3	3.34	16071	−0.23	2.16
30000027	B	3.8	3.84	16426	−0.82	3.05
1453928	C	3.75	3.91	16476	−0.73	3.14
30000029	B	4.38	4.42	16838	−0.46	3.12
30000031	B	4.8	5.04	17278	−0.03	2.66
30000033	B	5.3	5.54	17633	−1.17	2.42
30000035	B	5.8	6.04	17988	−0.73	3.1
1454124	C	6.15	6.31	18180	−0.52	3.24
30000037	B	6.36	6.6	18386	−1.04	3.18
30000040	B	6.84	7.08	18727	−1.22	2.85
1481130	B	7.09	7.34	18911	−1.97	2.53
30000041	B	7.3	7.54	19053	−3.37	3.75
1481038	B	7.34	7.58	19082	−6.3	3.13
1481134	B	7.5	7.74	19195	−0.72	2.81
30000043	B	7.8	8.04	19408	−1.24	2.84
30000045	B	8.2	8.44	19692	0.12	3.28
1368663	B	8.5	8.74	19905	−1.11	2.92
30000047	B	8.9	9.14	20189	−1.3	3.08
30000049	B	9.3	9.54	20473	−1.12	2.86
30000052	B	9.81	10.05	20835	−1.86	3.03
30000055	B	10.8	11.04	21538	−0.81	3.29
30000057	B	11.32	11.56	21908	−1.61	2.48
1368666	B	12.31	12.55	22610	−0.33	3.03
1368667	B	12.5	12.74	22745	−0.92	2.62
30000067	B	13.36	13.6	23356	−0.74	2.71
30000071	B	14.35	14.59	24059	−0.38	2.69
30000073	B	14.3	15.54	27615	−0.66	2.63
30000077	B	15.3	16.54	31358	−0.23	2.68
30000083	B	16.05	17.29	34165	−0.45	2.91
30000089	B	16.8	18.04	36935	−0.65	2.71
1368669	B	17.43	18.67	39293	−0.09	2.68
1368671	B	17.58	18.82	39758	−0.32	2.74
30000099	B	18.27	19.51	41866	−0.49	3
30000105	B	19.05	20.29	44249	−1.18	2.58
30000111	B	19.8	21.04	46541	−1.04	2.53
1453737	B	20.3	21.54	48069	−0.92	2.58
1368673	B	20.7	21.94	49291	−1.02	2.48

Table 4 (*Continued*).

Sample No.	Core	mbsf	mcd	Age model	$\delta^{13}C$	$\delta^{18}O$
1453803	B	21.27	22.51	51033	−0.59	2.56
1453805	B	21.8	23.04	52652	−0.22	3.01
1453807	B	22.27	23.51	54088	−1	2.92
1368679	C	24.27	23.99	55555	0.03	2.68
1453809	B	22.8	24.04	55708	−0.29	2.71
1453811	B	23.3	24.54	57236	−0.91	2.75
1453813	B	23.8	25.04	58763	−0.6	2.82
1454710	B	23.93	25.17	59161	−0.72	3.04
1453818	B	24.8	26.04	61819	−0.18	2.67
1453823	B	25.3	26.54	63347	−1.13	2.18
1453825	B	25.77	27.01	64783	−0.58	3.24
1453827	B	26.3	27.54	66402	−0.21	3.08
1453931	C	27.8	27.84	67319	−0.17	3.08
1453835	B	26.8	28.04	67930	−0.48	3.01
1453941	C	28.3	28.34	68847	−0.53	2.86
1453837	B	27.32	28.56	69519	−0.46	2.73
1453944	C	28.8	28.84	70375	0.08	2.88
1453946	C	29.3	29.34	71902	−0.66	2.94
1368684	B	28.55	29.79	73277	−0.43	2.94
1453948	C	29.8	29.84	73430	−0.54	2.79
1453951	C	30.3	30.34	74958	−0.33	3.15
1453953	C	30.8	30.84	76486	−0.42	3.09
1454760	C	31.3	31.34	78014	−0.82	2.82
1454008	C	31.8	31.84	79541	−0.06	2.87
1454010	C	32.3	32.34	81069	−0.68	2.87
1454012	C	32.8	32.84	82597	−0.05	3
1453839	B	33.3	34.61	88005	−0.5	2.96
1453841	B	33.82	35.13	89594	−0.95	2.8
1368686	C	35.62	35.66	91214	−0.86	2.44
1453861	B	35.85	37.16	95797	−0.56	3.02
1453865	B	36.85	38.16	98853	−0.36	2.7
1453873	B	37.83	39.14	101847	−0.05	2.97
1453877	B	38.83	40.14	104903	0.22	2.95
1453881	B	39.8	41.11	107867	0.11	2.89
1453886	B	40.81	42.12	110953	−0.33	2.79
1368688	B	41.69	43	113871	−0.07	2.67
1453890	B	42.11	43.42	115533	−0.13	2.69
1454014	C	42.65	43.65	116444	0.01	2.97
1368691	C	43.06	44.06	118067	−0.36	2.75
1454020	C	43.43	44.43	119531	0.15	2.83
1368693	C	43.73	44.73	120719	−0.14	2.47
1368695	C	43.84	44.84	121154	−0.39	2.38
1454024	C	43.92	44.92	121471	0.33	2.43
1454026	C	44	45	121787	−0.15	2.62
1368697	C	44.27	45.27	122856	0.42	2.61
1454032	C	44.6	45.6	124162	−0.08	2.43
1368699	C	44.99	45.99	125706	0.53	2.35
1454036	C	45.15	46.15	126340	−0.1	2.24
1368701	C	45.34	46.34	127092	−0.25	2.17
1454038	C	45.49	46.49	127685	0.17	2.34
1368702	C	45.64	46.64	128279	0.12	2.26
1454040	C	45.8	46.8	128912	0.34	2.62
1454042	C	46	47	129704	−0.3	2.45
1454044	C	46.2	47.2	130496	−0.12	2.09

Table 4 (*Continued*).

Sample No.	Core	mbsf	mcd	Age model	$\delta^{13}C$	$\delta^{18}O$
1454046	C	46.4	47.4	131287	−0.17	2.19
1454048	C	46.6	47.6	135050	−0.28	2.04
1454056	C	46.8	47.8	136053	−0.23	2.05
1454058	C	47	48	137056	0.05	2.28
1454071	C	46.38	48.64	140266	−1.05	2.58
1368806	C	46.53	48.79	141019	−1.31	2.64
1368808	C	46.78	49.03	142223	−0.9	2.86
1368810	C	46.96	49.22	143176	−1.43	2.74
1454073	C	47.15	49.41	144129	−1.19	2.87
1454075	C	47.35	49.61	145132	−1.09	2.71
1454077	C	47.55	49.81	146135	−1.02	2.75
1454100	C	47.8	50.06	147389	−1.39	2.41
1454102	C	48.05	50.31	148643	−1.08	3.08
1454104	C	48.3	50.56	149897	−1.09	2.77
1454106	C	48.7	50.96	151262	−1.83	3.43
1454108	C	49.1	51.36	151845	−1.02	2.21
1454110	C	49.6	51.86	152574	−1.95	2.9
1454112	C	51.1	53.36	154761	−1.51	3.2
1454120	C	52.6	54.86	156947	−1.46	2.68
1368814	C	54.45	56.71	159644	−0.87	3.07
1368816	B	58.8	62.58	168200	−1	2.99
1368820	C	61.64	64.6	171145	−0.92	2.8
1368822	C	62.58	65.54	172515	−0.69	2.81
1368824	C	63.3	66.26	173565	−0.41	2.58
1481084	C	66	71	180474	−1.05	3.01
1369006	C	67.35	72.35	182427	−0.51	3.05
1368828	B	67.33	72.64	182850	−0.65	2.96
1481086	C	68.89	73.89	184672	−0.65	3.15
1481090	C	70.39	75.39	186859	−0.83	2.87
1481094	C	71.82	76.82	191965	−1.18	2.51
1481098	C	73.25	78.25	198414	−0.52	3.05
1368830	C	73.37	78.37	198955	−0.49	2.91
1481050	C	74.87	79.57	205828	0.28	2.94
1481102	C	74.75	79.75	206861	−0.41	2.7
1481052	C	76	80.7	212311	−0.56	2.59
1481054	C	76.9	81.6	217475	−0.17	3
1511281	B	75.85	81.86	218967	−0.59	2.06
1368834	B	75.9	81.91	219254	−0.02	2.4
1481056	C	77.5	82.2	221115	−0.53	1.65
1511282	B	76.35	82.36	222231	−0.58	1.62
1368839	B	76.42	82.43	222719	−0.25	2.05
1481058	C	77.86	82.56	223625	−0.72	2
1511283	B	76.85	82.86	225717	−0.58	3.1
1368836	B	76.94	82.95	226344	−1.16	2.63
1481060	C	78.4	83.1	227390	−0.82	2.45
1511286	B	77.25	83.26	228505	−0.77	3.05
1481062	C	79	83.71	231643	−0.99	2.63
1511287	B	77.85	83.86	232688	−0.17	3.05
1368844	C	81.94	86.64	277000	−0.78	2.75
1481070	C	82.46	87.16	282461	−0.76	2.87
1481072	C	83.46	88.15	292858	−1.28	2.55
1481074	C	83.96	88.67	298320	−0.3	2.79
1481064	B	80.8	89	301653	−0.13	2.56
1481066	B	81.26	89.46	306125	0.04	2.44

Table 4 (*Continued*).

Sample No.	Core	mbsf	mcd	Age model	$\delta^{13}C$	$\delta^{18}O$
1481068	B	81.83	90.04	311764	−0.07	1.96
1511290	B	82.23	90.43	315556	0.46	2.56
1368951	B	82.66	90.86	319736	−0.3	2.55
1511291	B	83.12	91.32	324208	−0.63	2.46
1511292	B	83.62	91.82	329069	0.01	2.61
1368964	B	84.05	92.25	333250	−0.04	2.55
1511293	B	84.92	93.12	336549	−0.21	2.14
1368967	B	85.82	94.01	338546	−0.55	2.29
1368969	B	87.11	95.31	341464	−0.22	2.64
1368972	B	89.01	97.21	349577	−0.9	2.74
1369091	B	90.68	100.12	370000	−0.18	2.94

See accompanying text for analytical details.

and is caused by the particular oceanographic controls which have operated at the site.

5.3. Reflectance and γ-ray logs

The γ-ray emission and colour reflectance logs exhibit variability which is generally in phase with the climatic cyclicity delineated by the isotope curves, including most of the shorter interval fluctuations, but at higher resolution. Interglacial and other warm intervals are characterised by heavy $\delta^{13}C$ and high reflectance measurements, and low γ-ray and light $\delta^{18}O$. Conversely, glacial periods exhibit light $\delta^{13}C$ and low reflectance measurements, and high γ-ray and heavy $\delta^{18}O$ (Figs. 4 and 5).

This pattern is not unexpected. The γ-ray signal, responding to the presence of radiogenic elements such as K, U and Th, is a proxy for clay content, which was delivered to Site 1119 in enhanced quantities during cool periods because of lower sea levels and a nearby shoreline. Similarly, the colour reflectance is closely related to the carbonate content of the sediment (Millwood et al., 2003). In 1119 muds, carbonate is present mostly as planktonic microfossils which are concentrated in the warmer core intervals. Therefore, reflectance peaks (highs) and γ-ray peaks (lows, as plotted) both tend to be associated with the presence of foraminifera-rich sand beds (Figs. 4 and 5). This is part of a widespread pattern of G/I lithological variation in the Southwest Pacific, as previously reported by Griggs et al. (1983), Fenner et al. (1992), Nelson et al. (1993) and Carter et al. (2000). Overall, therefore, the γ-ray curve mainly reflects fluctuations in riverine sediment supply (which is a function of shoreline proximity, in turn controlled by sea level and climate), and the reflectance scale is a proxy for pelagic carbonate production.

A number of isolated γ-ray lows (represented as peaks on Fig. 4) stand out against the overall background match between the 1119 γ-ray log and the south polar Vostok climate record. We have labelled these anomalies Ga 1–4 and Gb 1–2. That matching or analogous features are absent from the oxygen isotope record confirms that these parts of the γ-curve reflect a local history rather than global oceanography. Possibly the gradually increasing and abruptly terminated γ-ray cycles each correspond to the gradual departure and sudden return of sediment focusing agents such as river mouths or frontal systems. Alternatively, they may mark a dwindling fluvial sediment input caused by increasing aridity, and hence reduced river outflow, during successive glacial pulses. Alternatively again, they may represent the dilution of a constant background terrigenous sediment component by biopelagic carbonate produced by increased surface productivity, an interpretation which is supported by the matching of most of these γ-lows with measures of higher carbonate percentage (reflectance) and productivity ($\delta^{13}C$). Their precise origin notwithstanding, however, the major glacial period γ-event cycles Ga 1–4 and Gb 1–2 are grouped

with a periodicity of ~5–10 kyr. In contrast to the six numbered γ-anomalies, the match between the Vostok climate curve and the γ-pattern outside of periods of peak glaciation demonstrates that in general the 1119 γ-curve closely reflects Antarctic, if not global, climate change.

6. General discussion: palaeoceanographic models

Most of the matters discussed above relate to the changing nature of the surface water masses which bathed Site 1119, and ultimately to climate change. It remains to assess the effect that these changes, especially those wrought by the changing position of the STF, exercised on the seabed and thereby on stratigraphic accumulation at Site 1119.

6.1. Interglacial graded sand–mud beds

Today, at interglacial highstand, Site 1119 is situated a little below storm wave base, and in a position of relatively low seabed current energy. The location is just downslope from the core of the STF frontal current and upslope from SAMW–AAIW drift influence, though possibly still just within the upper edge of this flow. Accordingly, the seabed at the site is mud, which was known from pre-Leg 181 cores to comprise the upper part of a sharp-based, graded, sand-mud rhythm of Holocene age. The early interglacial shelly sand at the base of this thin rhythm (S-1; Table 1) requires higher energy conditions for its deposition than exist at the modern seafloor. We infer, therefore, that sustained 40+ cm/s currents – capable of eroding the mud substrate, transporting fine sand, and conducive to the filter feeding benthos present in the basal Holocene sand (*Tawera*, *Neothyris*) – must have characterised a brief period during the latest Pleistocene and early Holocene, between ~12.9 and 9.5 ka. The initiating current flow was vigorous enough, and lasted long enough, to cause seabed erosion and allow the establishment of a firmground infauna of *Chondrites* burrowers. Because the shelly sand is completely enclosed within lower energy, muddy sediment, it must represent both the inception (at the sharp base) and then decline (over the graded top) of the causatory current. Similar sharp-based, graded shelly sands enclosed in silty clay occur also within the basal sediments of interglacials MIS 5 (S-5c) and MIS 7.5 (S-7d), and perhaps also MIS 9.3 (S-9c) (Table 1; Fig. 4). The two pre-Holocene basal interglacial sand beds are each overlain by similar sand beds (S-5b and S-7c, respectively), suggestive of a later phase of waxing and waning of the causatory current. Similar groups of thin sandy beds occur within interglacial horizons throughout the upper 400 m of the Site 1119 core, where they have been shown to contain temperate-water planktic foraminifera including *Orbulina universa*, *Globoratalia inflata* and *G. truncatulinoides* (Hayward et al., in: Carter et al., 1999), thus linking them with STW flow.

These factors considered, the most likely explanation for the early interglacial shelly sands is that they mark phases of northeastward flow along the STF as it came to be located near Site 1119 towards the end of each post-glacial sea-level rise. During the cutting of the erosion surface beneath the lowest sand in each interglacial packet, the core of frontal flow lay near the site, whereas during the peak interglacial sea-level high which followed a few thousand years later the front had moved further shoreward, leaving Site 1119 'drowned' in deeper (SAW) water where mud accumulation recommenced to form the upper part of the basal graded sand–mud packet (Fig. 8, upper). After the MIS 1–2 transition, peak interglacial frontal flow became concentrated inboard and upslope from Site 1119, in the vicinity of the outer shelf platform–shelf edge–upper slope where shell hashes which reflect strong current activity are exposed at the seabed today (cf. Carter et al., 1985; Orpin et al., 1998). The higher sand–mud bed in each of the older interglacial couplets may represent the subsequent (end-interglacial) seaward movement of the front across the site (Fig. 8, middle).

6.2. Glacial sediments: strengthened frontal gradients and upwelling

An important aspect of the Site 1119 record is that intervals of thin beds of graded sand–mud

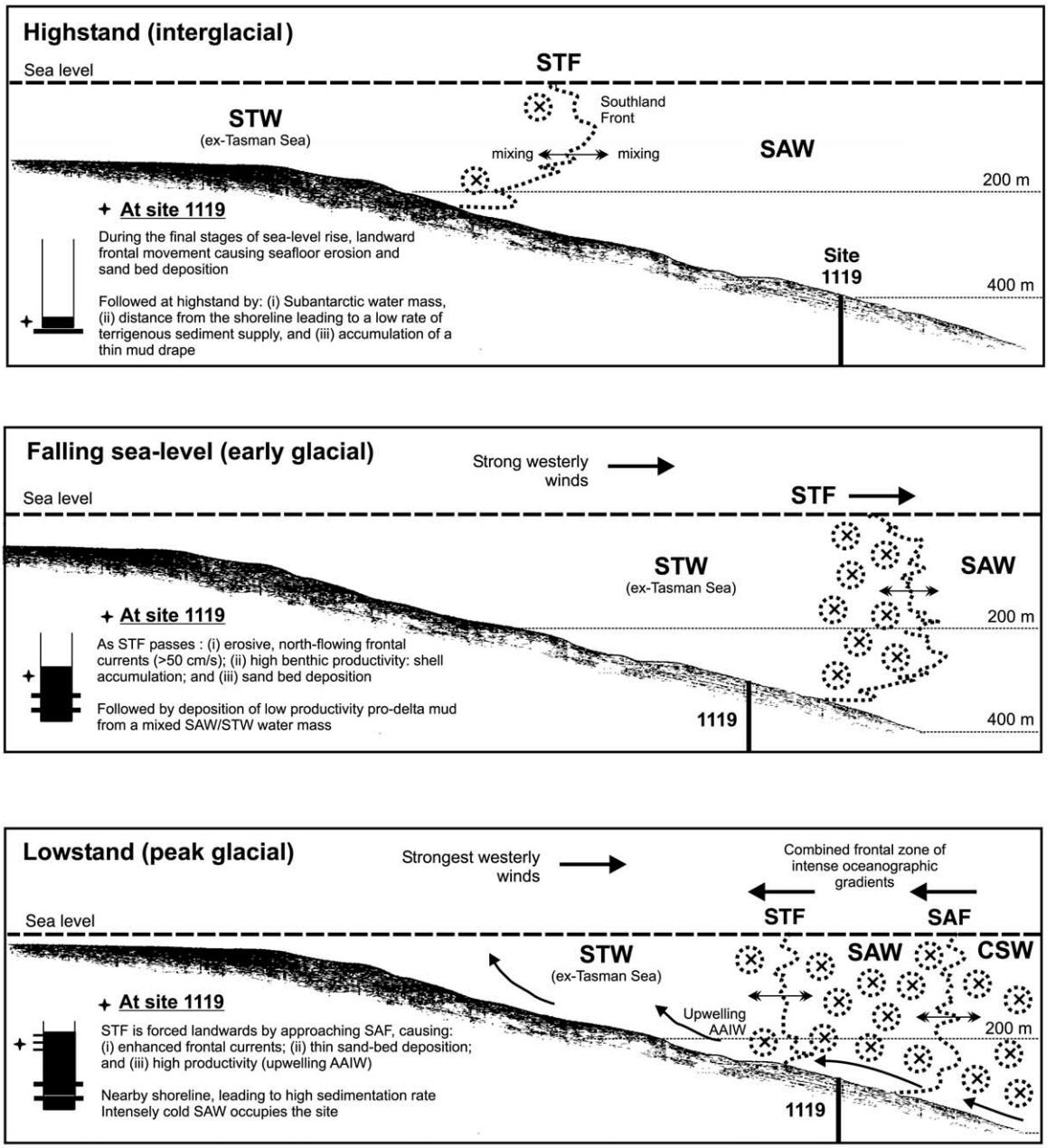

Fig. 8. Cartoon reconstructions of the oceanographic setting of Site 1119 during late post-glacial transgression and highstand (upper); during early glacial falling sea level and regression (middle); and at peak glacial lowstand (lower). Dotted circles depict northerly currents associated with the Subtropical (STF) and Subantarctic (SAF) fronts. STW, Subtropical Surface Water; SAW, Subantarctic Surface Water, CSW, Circumpolar Surface Water. See text for detailed discussion.

occur within peak glacial, as well as interglacial, intervals. These sands or shell concentrations are similar to but thinner than their interglacial analogues, and may be rich in carbonate benthos including particularly *Tawera*, serpulids and bryozoa. The glacial beds too show a strong signature of low γ-ray and high colour reflectance values (Fig. 4), including the Ga 1–4 and Gb 1–2 events, but exhibit no particular stable isotope signature apart from bearing a general association with the peak glacial band of $\delta^{13}C$ AAIW signature.

For the same reasons we considered above in our discussion of interglacial sands, we interpret the glacial sand-bed events as also representing the waxing and waning of bottom currents which were capable of transporting fine sand. There are three possible candidate currents. First, and as for their interglacial analogues, the glacial sands may represent phases of STF activity, and indicate the periodic influence of the Southland Front across Site 1119. Second, though during glaciations Site 1119 was situated at its minimum depth during a G/I cycle (MIS 2, ~250 m; MIS 6, ~300 m), it is possible that this lay within the top of a zone of glacially-expanded SAMW contour-current activity. An erosional-based, sand–mud, fining-upward cycle could be produced by the upslope and then downslope movement of the upper edge of the SAMW drift zone, perhaps driven by climatic intensifications in the subantarctic source areas of SAMW (cf. Lynch-Stieglitz et al., 1994). Third, the continental slope of eastern South Island may have been subjected to strengthened upwelling during glacials and stadials (e.g. Nelson et al., 2000). Given the northeast direction of the coastline, northerly winds today drive offshore Ekman transport, and upwelling, as reported by Heath (1972b, 1975). The currents associated with any such upwelling would at least augment, and might have dominated, sediment drift transport on the slope. By way of an example, major slope drifts deposited from upwelling currents have been documented along the west African coast (Seranne and Abeigne, 1999). Finally, the occurrence of a major MIS 6 negative oxygen isotope anomaly in the planktic (but not benthic) record at DSDP 594, which is matched at Site 1119 by the Gb 1–2 γ-ray events, indicates that the process which caused these anomalies was associated with surface waters, and extended at least 200 km offshore.

Taking these factors into consideration, and adopting an interpretation previously suggested by Nelson et al. (1993, 2000) and Weaver et al. (1998), it seems likely that the peak-glacial sand beds and their associated features were deposited from currents created by the coalescence of the STF and SAF into a single enhanced frontal system (Fig. 8, lower). An analogous merging of the SAF and Antarctic Polar Front occurs intermittently today in eastern Drake Passage (Peterson and Whitworth, 1989). It is established that a significant northward movement in the position of the SAF occurred in the Southwest Pacific during glaciations (e.g. Nelson et al., 1993; Wells and Okada, 1997; Weaver et al., 1997, 1998). At the same time, in the open Indian and Tasman Oceans, the STF also moved several degrees north (Howard and Prell, 1992; Wells and Connell, 1997), whereas east of South Island the STF was forced southeast by the interaction of bathymetry and a lowered sea level. The result of these frontal movements, at least within the Bounty gyre east of South Island, was that the SAF and STF came into close proximity, creating a combined SAF–STF zone of strongly enhanced oceanographic gradients. LGM temperatures were reduced to as low as 6°C summer and 2°C winter (Barrows et al., 2000), which correspond to modern polar frontal zone levels. Noting the relatively shallow 250 m water depth at Site 1119 during the peak of the last glaciation, we sugggest that the glacial sand beds represent the influence at the seabed of strongly enhanced current flows which developed along the combined SAF–STF during the glacial climax. As the climate deteriorated into a glacial maximum, and cold subantarctic and antarctic waters encroached strongly from the south towards the 'trapped' STF off eastern South Island, current flows of at least 40 cm/s expanded landwards from the front and impinged upon the bottom. During the final and deepest phases of glaciations MIS 6.2 and MIS 2, the oceanographic gradients became so strong that the STF itself was forced landwards by their effect (Fig. 7).

A $\delta^{13}C$ AAIW–CDW signal, strongly fluctuat-

ing $\delta^{18}O$ values, and the strong dissolution of planktic foraminifera (which occurs in several piston-cores nearby to Site 1119; Weaver et al., 1998) together characterise the several thousand year long peaks of MIS 2 and MIS 6.2 off eastern South Island. These features are consistent with upwelling of AAIW and upper CPDW, which may have accompanied strengthened frontal flows and movement during glaciation. Enhanced productivity which has previously been associated with MIS 2 upwelling at site 594 is apparent in that site's organic carbon record (Kowalski and Meyers, 1997), and may be represented at Site 1119 by the rich benthic fauna which occurs in the MIS 2 shelly and sand intervals. Finally, for these brief periods of maximum glaciation, it is possible that the STF in the Tasman Ocean migrated north sufficiently far to greatly reduce or altogether cut-off the supply of STW around the southern end of South Island. Thus at peak glaciations, waters across the entire eastern New Zealand plateau may have been fed entirely by cold surface SAW and upwelling AAIW–CPDW.

7. Conclusions

Today, ODP Site 1119 is situated a short distance downslope from the shelf edge of eastern South Island, New Zealand, in a water depth of 395 m. The site lies just seawards of the Subtropical Front (STF), and contains an expanded stratigraphic record of late Quaternary oceanographic change which can be correlated with the climatic record contained in the Vostok ice core. Based on the time scale developed from this correlation, we draw the following main conclusions.

(1) The upper 86.19 mcd of Site 1119 comprises upper slope clinoform strata deposited in the last 252 kyr, during marine isotope stages (MIS) 1–8. The underlying sediments down to 100 mcd, beneath a ~25 kyr-long downlap unconformity, represent MIS 8.5–10 (~277–370 ka) and consist of sediment drifts deposited from subantarctic mode water.

(2) Interglacials MIS 5, 7 and 9 are represented by silty clays which encompass two or more 5–65-cm-thick, sharp-based, *Chondrites*-burrowed, olive grey, graded, fine sands–muds. The sands are shelly (especially *Tawera*), and conspicuously rich in foraminifera, including temperate water forms (*Orbulina universa*, *Globorotalia inflata* and *G. truncatulinoides*). The intervening micaceous MIS 2, 6, 8 and 10 glacial muds may be cm-scale bedded, but are more usually massive and bioturbated; they contain the cold-water scallop *Zygochlamys delicatula*, and an enhanced siliceous and impoverished calcareous microfauna.

(3) The major glacial/interglacial (G/I) cyclicity at Site 1119 is well manifest in the stable isotope, γ-ray and % carbonate (reflectance) records. Warmer (sandy) intervals are characterised by heavy $\delta^{13}C$ and high carbonate, and low γ-ray and light $\delta^{18}O$; whereas colder (mostly mud) intervals exhibit light $\delta^{13}C$ and low carbonate, and high γ-ray and heavy $\delta^{18}O$. In addition, the $\delta^{13}C$ values distinguish the presence of subtropical water (STW; $\delta^{13}C = -0.8$ to -1.2‰), subantarctic water (SAW; $\delta^{13}C = 0.5$ to -0.5‰) and upwelled circumpolar deep water (CDW; $\delta^{13}C = -0.1$ to -0.15‰), and reflect the movements of these water masses during G/I cycling.

(4) During the Holocene and MIS 5.5 interglacials, the depth at Site 1119 was 395 m and ~350 m, respectively, the shoreline lay 80 km to the west, and the broad shelf was ventilated by the warm Southland Current, the seaward edge of which (the STF) lay inboard of the site and near the edge of the shelf. During such interglacials, transgressive shelly sand followed by highstand mud accumulated at low rates of ~5–25 cm/kyr, on an upper slope which was bathed in low salinity (34.2‰) SAW.

(5) As climatic cooling progressed, the falling sea level caused a narrowing of the shelf and the seawards movement of the STF across Site 1119, which for the majority of glacial period time lay landward of the front under more saline (34.8‰) STW. At the same time, during the last glacial lowstand the shoreline moved to within 15 km of Site 1119, which then lay at a depth of ~300 m. High sedimentation rates >100 cm/kyr resulted from the direct delivery nearby of river-borne sediment.

(6) During recent glacial maxima, the north-moving SAF came to be located close to eastern South Island, causing displacement of the STF landwards across Site 1119 and the development of a combined STF–SAF frontal zone of intense oceanographic gradients. Site 1119 lay within this frontal zone, where flows were accelerated by the temperature gradients to the degree that they impinged on the seabed. The longitudinal frontal currents reached at least 40 cm/s in waters down to ~250 m deep, emplacing thin beds of very fine sand which are marked on logs by conspicuous γ-ray (mud content) lows and reflectance (carbonate) highs.

Acknowledgements

The completion of this research was significantly delayed by a period of ill-health of the senior author. In such circumstances, R.M.C. is particularly grateful for the patience and support extended to him at that time by senior ODP colleagues Nick McCave, Lionel Carter and Bruce Hayward, and for the encouragement of Stewart Greenhalgh who provided facilities and research support at the University of Adelaide. We thank warmly the shipboard participants in ODP Leg 181 for their help with data collection. We also thank Sarah Harris, Graham Weedon, Will Howard, Cam Nelson, Basil Stanton, and Ken Ridgway for their willing help and advice, Alan Chappell, Yvonne Bone and Dave McKirdy for access to analytical and isotope facilities, ODP–TAMU curator Phil Rumford for his help with the provision of samples, David Fink (ANSTO) for help with provision of AMS radiocarbon dates, and Bernhard Weninger for advice regarding the use of the CALPAL radiocarbon calibration programme. Financial support for the research was provided by the Australian Research Council, under Special Investigator Grant A-39805139, and the Australian Institute of Nuclear Science and Engineering (AINSE) Grant 03/17. Finally, we thank referees Cam Nelson and Tim Naish for their helpful and patient critical advice on the draft manuscript.

References

Andrews, P.B., 1973. Late Quaternary continental shelf sediments off Otago Peninsula, New Zealand. N.Z. J. Geol. Geophys. 16, 793–830.

Bard, E., Hamelin, B., Arnold, M., Montaggioni, L., Cabioch, G., Faure, G., Rougerie, F., 1996. Deglacial sea-level record from Tahiti corals and the timing of global meltwater discharge. Nature 382, 241–244.

Barrows, S.T., Juggins, S., De Deckker, P., Thiede, J., Martinez, J.I., 2000. Sea-surface temperatures of the southwest Pacific Ocean during the Last Glacial Maximum. Paleoceanography 15, 95–109.

Broecker, W.S., van Donk, J., 1970. Insolation changes, ice volumes and the O^{18} record in deep-sea cores. Rev. Geophys. Space Phys. 8, 169–188.

Browne, G.H., Naish, T.R., 2003. Facies development and sequence architecture of a late Quaternary fluvial–marine transition, Canterbury Plains and shelf, New Zealand: Implications for forced regressive deposits. Sediment. Geol. 158, 57–86.

Burling, R.W., 1961. Hydrology of circumpolar waters south of New Zealand. N.Z. DSIR Bull. 143, 1–66.

CALPAL, 2003. The Cologne Radiocarbon Calibration and Paleoclimate Research Package, Universitat zu Koln (http://www.calpal.de/).

Carter, L., 1975. Sedimentation on the continental terrace around New Zealand: A review. Mar. Geol. 19, 209–237.

Carter, L., Heath, R.A., 1975. Role of mean circulation, tides and waves in the transport of bottom sediment on the New Zealand continental shelf. N.Z. J. Mar. Freshw. Res 9, 423–438.

Carter, L., Herzer, R.H., 1979. The hydraulic regime and its potential to transport sediment on the Canterbury continental shelf. NZOI Mem. 83, 1–33.

Carter, L., McCave, I.N., 1997. The sedimentary regime beneath the deep western boundary current inflow to the southwest Pacific Ocean. J. Sediment. Res. 67, 1005–1017.

Carter, L., Neil, H.L., McCave, I.N., 2000. Glacial to interglacial changes in non-carbonate and carbonate accumulation in the SW Pacific Ocean, New Zealand. Palaeogeogr. Palaeoclimatol. Palaeoecol. 162, 333–356.

Carter, R.M., 1988. Post-breakup stratigraphy of the Kaikoura Synthem (Cretaceous–Cenozoic), continental margin, southeastern New Zealand. N.Z. J. Geol. Geophys. 31, 405–429.

Carter, R.M., Norris, R.J., 1976. Cainozoic history of southern New Zealand: An accord between geological observations and plate-tectonic predictions. Earth Planet. Sci. Lett. 31, 85–94.

Carter, R.M., Carter, L., Williams, J., Landis, C.A., 1985. Modern and relict sedimentation on the Otago continental shelf. NZOI Mem. 93, 1–43.

Carter, R.M., Carter, L., Johnson, D.P., 1986. Submergent shorelines in the SW Pacific: Evidence for an episodic post-glacial transgression. Sedimentology 33, 629–649.

Carter, R.M., Carter, L., McCave, I.N., 1996. Current con-

trolled sediment deposition from the shelf to the deep ocean: The Cenozoic evolution of circulation through the SW Pacific gateway. Geol. Rundsch. 85, 438–451.
Carter, R.M., McCave, I.N., Richter, C., Carter, L. et al., 1999. Southwest Pacific Gateways, Sites 1119–1125. Proc. ODP Init. Rep. 181, 1–112 (CD-ROM).
Charles, C.D., Fairbanks, R.G., 1992. Evidence from Southern Ocean sediments for the effect of North Atlantic deep-water flux on climate. Nature 355, 416–419.
Charles, C.D., Lynch-Stiglitz, J., Ninnemann, U.S., Fairbanks, R.G., 1996. Climate connections between the hemisphere revealed by deep sea sediment core/ice core correlations. Earth Planet. Sci. Lett. 142, 19–27.
Chiswell, S.M., 1994. Variability in sea surface temperature around New Zealand from AVHRR images. N.Z. J. Mar. Freshw. Res. 28, 179–192.
Chiswell, S.M., 1996. Variability in the Southland Current, New Zealand. N.Z. J. Mar. Freshw. Res. 30, 1–17.
Clark, P.U., Alley, R.B., Keigwin, L.D., Licciardi, J.M., Johnsen, S.J., Wang, H., 1996. Origin of the first global meltwater pulse following the last glacial maximum. Paleoceanography 11, 563–577.
Cutler, K.B., Edwards, R.L., Taylor, F.W., Cheng, H., Adkins, J., Gallup, C.D., Cutler, P.M., Burr, G.S., Bloom, A.L., 2003. Rapid sea-level fall and deep-ocean temperature change since the last interglacial period. Earth Planet. Sci. Lett. 206, 253–271.
Dell, R.K., 1956. The archibenthal mollusca of New Zealand. N.Z. Dom. Mus. Bull. 18, 1–235.
Dudley, W.C., Nelson, C.S., 1989. Quaternary surface-water stable isotope signal from calcareous nannofossils at DSDP Site 593, southern Tasman Sea. Mar. Micropaleontol. 13, 353–373.
Fenner, J., Carter, L., Stewart, R., 1992. Late Quaternary paleoclimatic and paleoceanographic change over northern Chatham Rise, New Zealand. Mar. Geol. 108, 383–404.
Fleming, C.A., 1944. Molluscan evidence of Pliocene climatic change in New Zealand. R. Soc. N.Z. Trans. 74, 207–220.
Flower, B.P., Kennett, J.P., 1995. Biotic responses to temperature and salinity changes during last deglaciation, Gulf of Mexico. In: Effects of Past Global change on Life. National Research Council, Washington, DC, pp. 209–220.
Fulthorpe, C.S., Carter, R.M., 1991. Continental shelf progradation by sediment drift accretion. Geol. Soc. Am. Bull. 103, 300–309.
Garner, D.M., Ridgway, N.M., 1965. Hydrology of New Zealand Offshore Waters. N.Z. Oceanogr. Inst. Mem. 12.
Gray, F.L., 1993. The Karitane Canyon: A Submarine Valley Cut into the Otago Continental Shelf. Unpubl. MSc. Thesis, University of Otago, 150 pp.
Griffiths, G.A., Glasby, G.P., 1985. Input of river-derived sediment to the New Zealand continental shelf, I. Mass. Estuar. Coast. Shelf Sci. 21, 773–787.
Griggs, G.B., Carter, L., Kennett, J.P., Carter, R.M., 1983. Late Quaternary marine stratigraphy southeast of New Zealand. Geol. Soc. Am. Bull. 94, 791–797.
Hall, I.R., McCave, I.N., Shackleton, N.J., Weedon, G.P., Harris, S.E., 2001. Intensified deep Pacific inflow and ventilation in Pleistocene glacial times. Nature 412, 809–812.
Heath, R.A., 1972a. The Southland Current. N.Z. J. Mar. Freshw. Res. 6, 497–533.
Heath, R.A., 1972b. Oceanic upwelling produced by northerly winds on the north Canterbury coast. N.Z. J. Mar. Freshw. Res. 6, 343–351.
Heath, R.A., 1975. Oceanic Circulation and Hydrology off the Southern Half of South Island, New Zealand. N.Z. Oceanogr. Inst. Mem. 72, 36 pp.
Heath, R.A., 1981. Oceanic fronts around southern New Zealand. Deep-Sea Res. 28, 547–560.
Heath, R.A., 1985. A review of the physical oceanography of the seas around New Zealand. N.Z. J. Mar. Freshw. Res. 19, 79–124.
Hellstrom, J., McCulloch, M., Stone, J., 1998. A detailed 31,000-year record of climate and vegetation change, from the isotope geochemistry of two New Zealand speleothems. Quat. Res. 50, 167–178.
Herzer, R.H., 1981. Late Quaternary stratigraphy and sedimentation of the Canterbury continental shelf, New Zealand. N.Z. Oceanogr. Inst. Mem. 89, 1–71.
Howard, W.R., Prell, W.L., 1992. Late Quaternary surface circulation of the southern Indian ocean and its relationship to orbital variations. Paleoceanography 7, 79–117.
Imbrie, J., Hays, J.D., Martinson, D.G., McIntyre, A., Mix, A.C., Morley, J.L., Pisias, N.G., Prell, W.L., Shackleton, N.J., 1984. The orbital theory of Pleistocene climate: Support from a revised chronology of the marine $\delta^{18}O$ record. In: Berger, A.L., et al. (Eds.), Milankovitch and Climate, Part 1, pp. 269–305.
Joris, O., Weninger, B., 2000. Radiocarbon calibration and the absolute chronology of the Late Glacial. Mem. Mus. Prehist. Ile de Fr. 7, 19–54.
Kennett, J.P., Ingram, B.L., 1995. Paleoclimatic evolution of Santa Barbara Basin during the last 20 k.y.: Marine evidence from hole 893A. Proc. ODP Sci. Res. 146, 309–325.
Kennett, J.P., Shackleton, N.J., 1975. Laurentide ice sheet meltwater recorded in Gulf of Mexico deep-sea cores. Science 188, 147–150.
Kowalski, E.A., Meyers, P.A., 1997. Glacial–interglacial variations in Quaternary production of marine organic matter at DSDP Site 594, Chatham Rise, southeastern New Zealand margin. Mar. Geol. 140, 249–263.
Lu, H., Fulthorpe, C.S., Mann, P., 2003. Three-dimensional architecture of shelf-building sediment drifts in the offshore Canterbury Basin, New Zealand. Mar. Geol. 193, 19–47.
Lynch-Stieglitz, J., Fairbanks, R.G., 1994. A conservative tracer for glacial ocean circulation from carbon isotope and palaeo-nutrient measurements in benthic foraminifera. Nature 369, 308–310.
Lynch-Stieglitz, J., Fairbanks, R.G., Charles, C.D., 1994. Glacial–interglacial history of Antarctic Intermediate Water: Relative strengths of Antarctic versus Indian Ocean sources. Paleoceanography 9, 7–29.
Mackensen, A., Rudolph, M., Kuhn, G., 2001. Late Pleisto-

cene deep-water circulation in the subantarctic eastern Atlantic. Glob. Planet. Change 30, 197–229.

Matsumoto, K., Lynch-Stieglitz, J., 1999. Similar glacial and Holocene deep water circulation inferred from southeast Pacific benthic foraminiferal carbon isotope composition. Paleoceanography 14, 149–163.

Millwood, L.D., Hawkins, D.L., Wells, S.M., 2003. Utilizing color reflectance as a carbonate concentration proxy: Data Report. ODP Leg 181 Sci. Rep. (in press).

Morris, M., Stanton, B., Neil, H., 2001. Subantarctic oceanography around New Zealand: Preliminary results from an ongoing survey. N.Z. J. Mar. Freshw. Res. 35, 499–519.

Nelson, C.S., Cooke, P.J., Hendy, C.H., Cuthbertson, A.M., 1993. Oceanographic and climate changes over the past 150,000 years at Deep Sea Drilling Project Site 594 off southeastern New Zealand, southwest Pacific Ocean. Palaeoceanography 8, 435–458.

Nelson, C.S., Hendy, C.H., Cuthbertson, A.M., Jarrett, G.R., 1986. Late Quaternary carbonate and isotope stratigraphy, subantarctic Site 594, southwest Pacific. In: Kennett, J.P., von der Borch, C.C., et al. (Eds.), DSDP Init. Rep. Leg 90, 1425–1436.

Nelson, C.S., Hendy, I.L., Neil, H.L., Hendy, C.H., Weaver, P.P.E., 2000. Last glacial jetting of cold waters through the Subtropical Convergence zone in the Southwest Pacific off eastern New Zealand. Palaeogeogr. Palaeoclimatol. Palaeoecol. 156, 103–121.

Orpin, A.R., 1997. Dolomite chimneys as possible evidence of coastal fluid expulsion, uppermost Otago continental slope, southern New Zealand. Mar. Geol. 138, 51–67.

Orpin, A.R., Gammon, P.R., Naish, T.R., Carter, R.M., 1998. Modern and ancient *Zygochlamys delicatula* shellbeds from New Zealand, and their sequence stratigraphic implications. Sediment. Geol. 122, 267–284.

Peterson, R.G., Whitworth, T., 1989. The Subantarctic and Polar Fronts in relation to deep water masses through the Southwestern Atlantic. J. Geophys. Res. 94, 10817–10838.

Petit, J.R. et al., 1999. Climate and atmostpheric history of the past 420,000 years from the Vostok ice core, Antarctica. Nature 399, 429–436.

Powell, A.W.B., 1950. Mollusca from the Continental Shelf, Eastern Otago. Auckland Inst. Mus. Rec. 4, 73–81.

Ridgway, K.R., Dunn, J.R., 2002. Mesoscale structure of the East Australian Current system and its relationship with topography (in press).

Sarnthein, M., Tiedemann, R., 1990. Younger Dryas-style cooling events at glacial terminations I–VI at ODP Site 658: Associated benthic $\delta^{13}C$ anomalies constrain meltwater hypothesis. Paleoceanography 5, 1041–1055.

Seranne, M., Abeigne, C.-R.N., 1999. Oligocene to Holocene sediment drifts and bottom currents on the slope of Gabon continental margin (west Africa). Consequences for sedimentation and southeast Atlantic upwelling. Sediment. Geol. 128, 179–199.

Shackleton, N.J., 2000. The 100,000-year ice-age cycle identified and found to lag temperature, carbon dioxide and orbital eccentricity. Science 289, 1897–1902.

Sikes, E.L., Samson, C., Guilderson, T.P., Howard, W.R., 2000. Old radiocarbon ages in the southwest Pacific Ocean during the last glacial period and deglaciation. Nature 405, 555–559.

Sokolov, S., Rintoul, S., 1999. Circulation of the Southwest Pacific: WOCE section P11, Papua New Guinea to Tasmania. WOCE Newslett. 36, 32–35.

Stanton, B.R., 1973. Circulation along the eastern boundary of the Tasman Sea. In: Fraser, R. (comp.), Oceanography of the South Pacific 1972. National Commission for UNESCO, Wellington, pp. 141–147.

Stanton, B.R., 1976. Circulation and hydrology off the west coast of the South Island, New Zealand. N.Z. J. Mar. Freshw. Res. 10, 445–467.

Stanton, B.R., Ridgway, N.M., 1988. An oceanographic survey of the subtropical convergence zone in the Tasman Sea. N.Z. J. Mar. Freshw. Res. 22, 583–593.

Stuiver, M., Reimer, P.J., Bard, E., Beck, J.W., Burr, G.S., Hughen, K.A., Kromer, B., McCormac, G., van der Plicht, J. (Eds.), INTCAL98 Radiocarbon age calibration, 24,0000–0 cal BP. Radiocarbon 40 (3).

Weaver, P.P.E., Carter, L., Neil, H., 1998. Response of surface watermasses and circulation to late Quaternary climate change, east of New Zealand. Paleoceanography 13, 70–83.

Weaver, P.P.E., Neil, H., Carter, L., 1997. Sea surface temperature estimates from the Southwest Pacific based on planktonic foraminifera and oxygen isotopes. Palaeogeogr. Palaeoclimatol. Palaeoecol. 131, 241–256.

Wells, P.E., Connell, R., 1997. Movement of hydrological fronts and widespread erosional events in the southwestern Tasman Sea during the late Quaternary. Aust. J. Earth Sci. 44, 105–112.

Wells, P.E., Okada, H., 1997. Response of nannoplankton to major changes in sea-surface temperature and movements of hydrological fronts over Site DSDP 594 (south Chatham Rise, southeastern New Zealand), during the last 130 kyr. Mar. Micropaleontol. 32, 341–363.

Wilson, K., Hayward, B., Scott, G., 2002. Paleoceanography of the Canterbury Bight: Planktic foraminiferal evidence for the last 1 million years from ODP 1119. Geol. Soc. N.Z. Annu. Conf. (Whangarei), Abstracts, p. 58.